

Article

Influence of Different Construction Methods on Lateral Displacement of Diaphragm Walls in Large-Scale Unsupported Deep Excavation

Hao-Wei Chiu¹, Chia-Feng Hsu^{2,*} , Fu-Huan Tsai³ and Shong-Loong Chen¹ 

¹ Department of Civil Engineering, National Taipei University of Technology, Taipei 10608, Taiwan; herciam.eu@gmail.com (H.-W.C.); f10391@ntut.edu.tw (S.-L.C.)

² Department of Civil Engineering, Chienkuo Technology University, Changhua City 500020, Taiwan

³ Huaku Development Co., Ltd., Taipei 110501, Taiwan; tim30151@gmail.com

* Correspondence: chiafeng1013@gmail.com

Abstract: This study examines the influence of different construction methods on the lateral displacement of diaphragm walls in large-scale, unsupported deep excavations. Using the three-dimensional finite element method (FEM) with PLAXIS 3D 2017 software, the research assesses how varying construction techniques impact wall stability, particularly in proximity to sensitive structures like metro systems. The project uniquely integrates peripheral top-down and central bottom-up approaches to minimize environmental disruption. Key focus areas include the roles of back-pull slabs, zoned excavation, and cross walls in reducing wall deformation. Findings reveal that zoned excavation significantly controls lateral displacement on longer site sides, enhancing adjacent structure safety and overall construction integrity. Back-pull slabs are shown to effectively decrease top wall deformation, thereby increasing structural stiffness. Moreover, despite their considerable length (nearly 60 m), cross walls play a crucial role in controlling lateral deformation along the excavation's length. These insights offer valuable guidance for future projects, especially in regions like Taiwan, where experience with such large-scale, unsupported excavations is limited.



Citation: Chiu, H.-W.; Hsu, C.-F.; Tsai, F.-H.; Chen, S.-L. Influence of Different Construction Methods on Lateral Displacement of Diaphragm Walls in Large-Scale Unsupported Deep Excavation. *Buildings* **2024**, *14*, 23. <https://doi.org/10.3390/buildings14010023>

Academic Editors: Yongqiang Zhou, Erdi Abi, Longlong Lv and Shaobo Chai

Received: 30 November 2023

Revised: 16 December 2023

Accepted: 17 December 2023

Published: 21 December 2023



Copyright: © 2023 by the authors. Licensee MDPI, Basel, Switzerland. This article is an open access article distributed under the terms and conditions of the Creative Commons Attribution (CC BY) license (<https://creativecommons.org/licenses/by/4.0/>).

Keywords: large-scale deep excavation; unsupported; FEM; zoned excavation; back-pull slab; cross wall

1. Introduction

This study explores the complexities of and innovative solutions for large-scale, unsupported deep excavations in Taiwan's urban environments. These excavations, essential for the development of high-rise buildings and extensive subterranean structures, are driven by the growing demand for space. Emphasizing the management of excavation projects that exceed 10,000 square meters, the study focuses on the 'Peripheral Top-Down and Central Bottom-Up' approach. Although this method is not widely used in Taiwan, it presents substantial benefits, including a reduced reliance on temporary supports, faster excavation processes, and the use of structurally robust diaphragm walls to maintain foundational stability effectively.

Employing Plaxis 3D 2017 for numerical analysis, the research corroborates its findings with field data, specifically evaluating the method's capacity to control wall deformation. This includes the strategic use of buttress walls, cross walls, and structural slabs in managing diaphragm wall deformation. A key aspect of the study is the detailed examination of back-pull slabs and the use of cross walls extending nearly 60 m, assessing their effectiveness in reducing wall deformation. The investigation, through both field monitoring and numerical simulation, seeks to determine the efficiency of these cross walls in mitigating deformation. The study compiles the various advantages of this construction technique, thereby providing valuable insights for future design practices and serving as a resource for academic research.

In summary, this study combines practical engineering case examples with monitoring data for validation. Currently, such cases are relatively rare in Taiwan. Therefore, it provides an excellent demonstration of design and construction for future large-scale, irregular, unsupported deep excavation projects in Taiwan. By referring to the various numerical scenario analyses and associated construction methods detailed in this case, the goal of achieving optimized design and construction can be accomplished.

Literature Review

• Peripheral Top-Down and Central Bottom-Up Method

The ‘Peripheral Top-Down and Central Bottom-Up’ method, highlighted in Liu’s Foundation Pit Engineering Handbook (second edition) [1], represents a sophisticated approach for managing ultra-large-area deep excavations, often covering areas beyond tens of thousands of square meters. This technique involves initially constructing a rigid ring beam slab around the excavation site’s perimeter. The process commences with central area excavation, moving downwards to the designated level, and is followed by upward construction that connects back to the peripheral ring slab. Meanwhile, the peripheral sections undergo a simultaneous process of layered excavation and top-down construction. This method is particularly effective for sites with a minimum of two basement levels and a polygonal excavation plan. Critical aspects include ensuring the peripheral ring slab’s width for optimal rigidity, angling the surrounding soil for stability, and preserving a significant central space for bottom-up construction once the top-down section is complete.

Lim and Ou’s [2] case studies of unsupported excavations in soft soil [2] show that buttress walls and internal structural slabs are often used in large-scale unsupported excavations to serve as a support structure system. This strategy effectively reduces both construction costs and timeframes. The final lateral displacement of the wall relative to the final excavation depth (ratio δ_{lm}/H_e) is observed to range between 0.27 and 0.55. For the longer sides of the excavation site, diaphragm walls exhibit translational movement at the wall’s toe, as depicted in Figure 1a, resulting in a cantilevered wall deformation. Conversely, on the shorter sides, the diaphragm walls show curvilinear deformation, with the maximum wall deformation occurring below the final excavation level, as illustrated in Figure 1b.

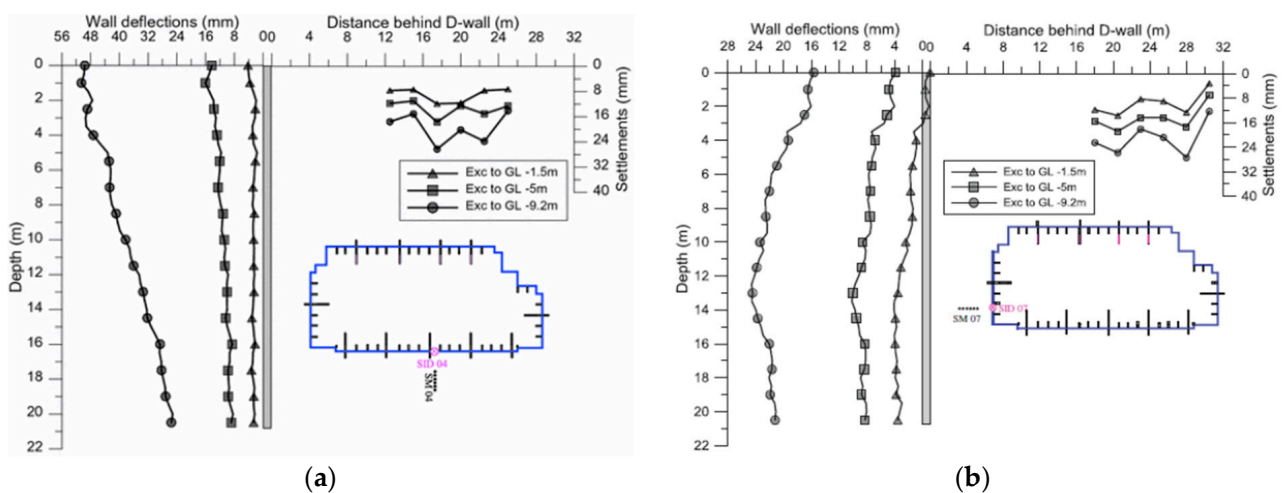


Figure 1. Monitoring curves for lateral wall deformation and ground settlement at the site: (a) longitudinal; (b) transverse (Lim and Ou [2]).

• Impact of Zoned Excavation

Ou [3] mentioned that for excavation sites using diaphragm walls as retaining walls, due to the arching effect of the concrete walls, the deformation and surface settlement at and near the corners where the diaphragm walls meet are relatively small. Additionally,

the deformation on the shorter sides of the excavation site is less than that on the longer sides. Zoned excavation utilizes this principle to reduce deformation of the retaining walls and surface settlement during excavation.

Jeng and Ho [4] conducted a simulation study focusing on a Taipei site using the Peripheral Top-Down and Central Bottom-Up method, primarily examining the stability and deformation of retaining walls during excavation. Their approach included both three-dimensional and simplified one-dimensional analyses for comparison. Findings indicated that the maximum deformation of diaphragm walls in the three-dimensional analysis closely aligned with actual field measurements, though variations in deformation patterns were noted. Comparisons between full area and zoned excavation revealed that zoned excavation, as per numerical simulations, significantly reduced the lateral displacement of the diaphragm wall bodies.

In a study by Li [5], the excavation process at Shanghai Xi Railway Station metro station was scrutinized. To safeguard the railway and subway systems, a zoned construction approach was proposed, incorporating the erection of several cross walls alongside necessary support structures. This technique partitioned the extensive deep excavation area into smaller, manageable zones. This phased and zoned construction method successfully mitigated conflicts between construction activities and railway operations. The outcomes showed that this approach effectively protected adjacent infrastructures, with maximum lateral wall displacements varying between $0.05\% H_e$ and $0.42\% H_e$, as depicted in Figure 2. This is within the range of $0.1\% H_e$ and $1.0\% H_e$ proposed by Wang et al. [6], where H_e is the final excavation depth. The study suggested that utilizing the Time-Space Effect (TSE) in phased and zoned construction techniques can aid in the control of deformation in deep excavations.

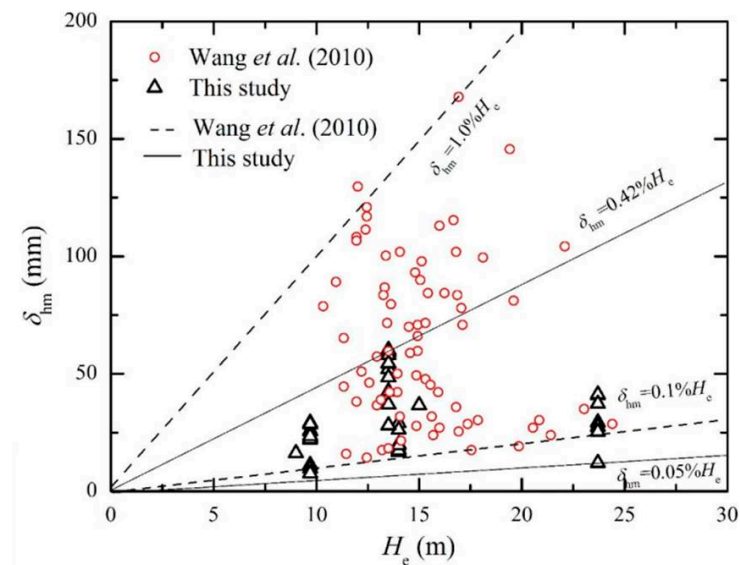


Figure 2. Graph showing the relationship between maximum wall displacement and excavation depth in the Shanghai area (Wang et al. [6]).

- **Lateral Deformation of Retaining Walls Due to Deep Excavation**

Clough and O'Rourke's research [7] delineates three distinct patterns of deformation in retaining walls during excavation projects: cantilever displacement, deep lateral inward displacement, and a combination of both. In deep excavations lacking top supports or countermeasures, the walls typically exhibit a cantilever-like displacement. This behavior is influenced by the depth-to-width ratio and the restraint provided by soil at penetration points. The study also notes that different types of soil, such as hard clay, residual soils, and sandy soils, result in varying degrees of ground surface settlement around these structures. It was found that, on average, the maximum lateral displacement of a wall is

approximately 0.2% of the excavation depth (H), seldom exceeding 0.5% H . Factors such as poor construction quality or insufficient wall depth could lead to excessive displacement. Particularly in softer clay layers, there is a notable correlation between wall displacement and excavation depth, linked to the safety factor against bottom heave. Ou et al. [8] further expand on this topic by discussing how the location of maximum lateral displacement in diaphragm wall bodies changes relative to the excavation depth. While the initial excavation phase predominantly causes cantilever displacement with maximum lateral displacement at the top of the wall, in later phases, this maximum displacement tends to occur closer to the excavation face's depth. According to a finite element method-based parameter analysis of deep excavation wall deformations conducted by Manna and Clough [9], which was compared with field monitoring results of deep excavations, several critical factors can be identified that influence the deformation behavior of deep excavation walls, including the safety factor against heave, the stiffness of the retaining wall and its support systems, the magnitude of support pre-stress, the excavation area's geometric shape, and the duration of the construction period.

Masuda et al. [10] took a broader approach, analyzing 52 excavation cases to identify key factors influencing excavation stability. They concluded that soil stiffness and support stiffness are primary influencers. Additionally, they identified 11 specific factors contributing to retaining wall deformation, including soil type and properties, wall and support stiffness, number and spacing of supports, support pre-stress, excavation method, wall length, ground improvement measures, excavation scale, groundwater conditions, and other concurrent construction activities. Notably, cross walls, which link diaphragm walls either on the north–south or east–west axes, serve as a crucial support system. These walls, typically reinforced below the excavation face and progressively removed during excavation, enhance rigidity, reduce wall deformation, and provide resistance against uplift. Wu et al. [11] focused on the application of cross walls in regions like Japan and Taiwan. Their research, involving 11 real cases with cross walls and 11 models without, found that cross walls significantly reduce wall displacement and ground surface settlement. They developed a simplified regression model for predicting the deformation of diaphragm wall bodies with cross walls. Their research highlights the corner effect in cross walls, akin to that in diaphragm walls, where displacement at the T-junction is minimal. The study also notes that the displacement profile of adjacent cross walls is similar to a pattern illustrated in their diagram, shown in Figure 3.

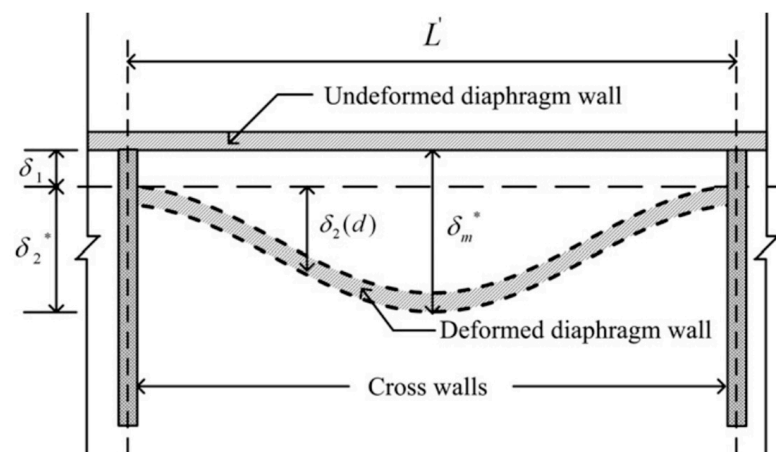


Figure 3. Wall displacement for excavation with cross walls (Wu et al. [11]).

In the figure, δ_m in general, denotes the maximum wall displacement, while $\delta_m(d)$ denotes the δ_m measured at a distance d away from the corner. This notation of d is needed because the corner effect shows that δ_m decreases with decreasing d . A special case of δ_m is $\delta_m\left(d = \frac{L'}{2}\right)$, denoted by δ_m^* , the maximum wall displacement at the middle.

• Application of Numerical Analysis in Deep Excavation Engineering

In their study, Do et al. [12] conducted a detailed analysis using the finite element method with PLAXIS software, focusing on a deep excavation project in soft soil that experienced three failures and one instance of excessive deformation. The research brought attention to a unique phenomenon dubbed “toe-kicking” occurring at the bottom end of the diaphragm wall. This phenomenon involves the soil situated behind the wall moving downward and forward into the excavated area. As a result, the embedded portion of the wall is compelled to move and bend toward the excavation area. The study observed that the maximum horizontal displacement happens at the toe of the wall, as depicted in Figure 4. Crucially, the occurrence of this toe-kicking phenomenon is conditional on specific angular relationships: it is not observed when α_1 is less than α_2 , but it does occur when α_1 exceeds α_2 . This finding adds a vital understanding of wall behavior and soil interaction in deep excavation scenarios, particularly in soft soil conditions.

$$\alpha_1 = \tan^{-1}\left(\frac{H_e}{D_{He} - D_o}\right) \quad (1)$$

$$\alpha_2 = \tan^{-1}\left(\frac{H_p}{D_{He+Hp} - D_{He}}\right) \quad (2)$$

where H_e : excavation depth; H_p : penetration depth; D_o : ground horizontal displacement; D_{He} : final excavation depth horizontal displacement; D_{He+Hp} : toe displacement of the wall.

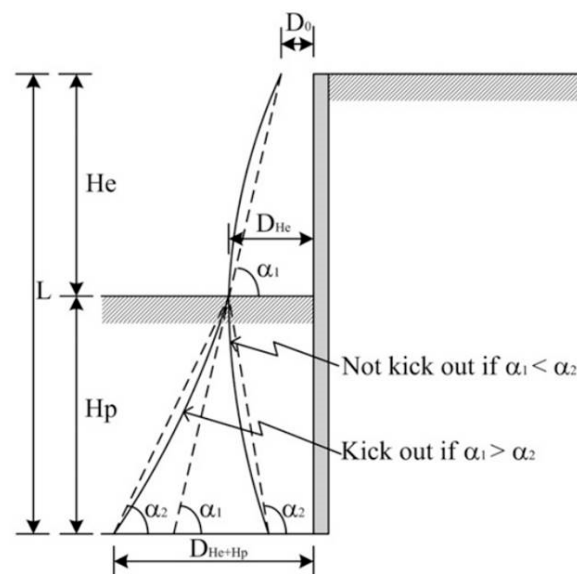


Figure 4. The toe-kicking phenomenon of the wall (Do et al. [12]).

Chheng et al. [13] undertook a comprehensive analysis of a deep excavation project in Bangkok through a three-dimensional finite element approach using PLAXIS 3D. This analysis, fine-tuned with data from both laboratory and field tests, aimed to draw a comparison between the simulated wall deformations and ground settlements in three dimensions against the conventional two-dimensional analyses and actual monitoring data. The study highlighted the limitations of two-dimensional methods, particularly their inability to account for the corner effect. In contrast, the three-dimensional model revealed distinct variations in lateral deformations along the longer and shorter sides of the excavation site, with an average difference of about 10%. A notable observation was the reduced wall movement near the excavation corners. The three-dimensional method’s primary advantage lies in its capacity to replicate construction sequences realistically, thereby providing more accurate predictions of wall deformation and ground settlement at different stages of construction.

Similarly, Chen et al. [14] utilized a 3D software tool to investigate the role of exterior struts in minimizing the maximum lateral deformation in the middle of diaphragm walls, particularly in soft ground excavations. The study, corroborated by field data from the Taipei 101 and Neihu basement projects, delved into how the geometry of buttress walls influences their stabilizing effect. While simplifying the problem to two dimensions is common, it often fails to capture the full picture, especially for nearly square excavation sites. The research suggests that for buttress walls, the optimal spacing should be less than double the depth of the excavation, with T-shaped designs proving more effective than I-shaped ones. The study also emphasized the importance of not removing these walls sequentially during excavation to ensure optimal stability of the diaphragm wall.

Hsiung et al. [15] conducted a case study on wall deformation in a major deep excavation project in central Jakarta, Indonesia. This study employed three-dimensional numerical simulations to analyze wall deformation and bending moments, comparing these results with those from two-dimensional simulations. The findings indicated a high level of consistency between the 2D and 3D results. Moreover, the corner areas in the 3D simulation displayed smaller displacements compared to plane strain conditions, aligning more closely with the actual conditions observed on site.

Lim et al. [16] introduced new metrics to assess the impact of wall deformation and ground settlement, as illustrated in Figure 5: the maximum deflection ratio (MDR), maximum settlement ratio (MSR), and deflection area ratio (DAR). These ratios are defined and calculated using Equations (3)–(5). This innovative approach offers a more nuanced understanding of the effects of wall deformation and ground settlement in deep excavation projects.

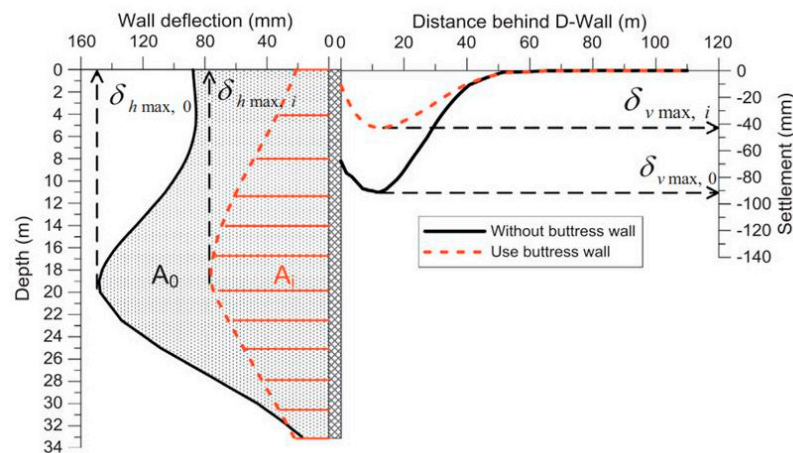


Figure 5. Illustration of parameters used for calculating MDR, MSR, and DAR values (Lim et al. [16]).

In this subsection, the performance of buttress walls is summarized and assessed quantitatively. Therefore, three parameters, namely, the maximum deflection ratio (MDR), the maximum settlement ratio (MSR), and the deflection area ratio (DAR), are proposed. The MDR, MSR, and DAR are defined as Equations (3)–(5):

$$\text{MDR} = \frac{\delta_{hm-0} - \delta_{hm-i}}{\delta_{hm-0}} \times 100\% \quad (3)$$

$$\text{MSR} = \frac{\delta_{vm-0} - \delta_{vm-i}}{\delta_{vm-0}} \times 100\% \quad (4)$$

$$\text{DAR} = \frac{A_0 - A_i}{A_0} \times 100\% \quad (5)$$

where:

- δ_{hm-0} = the maximum lateral wall deflection without buttress walls;

- δ_{lm-i} = the maximum lateral wall deflection with buttress walls;
- δ_{vm-0} = the maximum ground surface settlement without buttress walls;
- δ_{vm-i} = the maximum ground surface settlement with buttress walls;
- A_0 = the plane area of lateral wall deflection without buttress walls;
- A_i = the plane area of lateral wall deflection with buttress walls.

In their study of a deep excavation project in Singapore, Chuah [17] explored the use of an unsupported excavation method that incorporated internal buttresses and structural slabs, ideal for large-scale, enclosed excavations. This innovative approach led to a cantilever pattern in wall deformation due to the lack of internal supports. Chuah utilized the finite element method with PLAXIS modeling to analyze this. The study highlighted that, unlike the more traditional 2D analyses, the 3D analysis provided a comprehensive and accurate representation of the deformation patterns. This insight is particularly vital in unsupported conditions, where controlling lateral wall deformation is crucial to prevent significant ground settlement.

• Utilization of Corners

According to Ou [3], diaphragm walls exhibit an “arch effect” at corners due to their horizontal stiffness, leading to less deformation and surface settlement near these areas compared to the central sections. This contrasts with steel sheet piles and soldier piles, which, lacking this horizontal stiffness, do not demonstrate the same effect, resulting in similar deformations at corners and central sections. Therefore, in scenarios where a building is close to the excavation site’s corners or along its shorter side, using diaphragm walls as retaining structures can be advantageous to capitalize on this corner effect and better protect the surrounding environment.

• Large-Scale Deep Excavation

Liu et al. [18] reported on a massive 10.9–15.6 m deep, 70,500 m² irregular pit in Shanghai’s soft clay, excavated using the bottom-up method and supported by auger cast-in-place pile walls and concrete struts. The key findings include: (1) the prolonged construction and large pit scale resulted in maximum wall deflection and ground subsidence exceeding 0.86% of the final excavation depth (H_e), significantly higher than other Shanghai excavations and surpassing allowable deformation limits; (2) basal heave displayed a dome-shaped pattern with minimal distortion between adjacent columns, but maximum distortion between columns and retaining walls neared the 0.2% limit; (3) significant axial force discrepancies were noted, with some axial forces in diagonal struts being 15% over the design value due to the spatial effects of internal supports; (4) the surrounding pipelines showed three-dimensional deformation and significant settlement, with a maximum of 56 mm.

Liu et al. [19] studied an 18.4 m deep triangular foundation pit in soft clay, covering about 10,000 m², at Shanghai’s Hongqiao transportation hub. Key observations from the monitoring system during excavation include wall deflections, vertical wall and column movements, and ground subsidence. The pit’s unique triangular shape, with acute corners, resulted in deformation characteristics distinct from other metro station or rectangular excavations in Shanghai. These findings are crucial for designing and constructing special-shaped pits in complex environments.

Ren et al. [20] conducted a study on a large 25,720 m², 20 m deep foundation pit in Chengdu, China, excavated in 2012–2013. The monitoring process included observing column movements, deflections, internal stress, anchor cable forces, ground settlement, and water levels. Analysis of this excavation, along with ten others in Chengdu, provided key insights: the maximum column deflection generally occurs at the top, vertical movements stabilize after excavation, and anchor cable forces range from 20 to 70 kN. Notably, minimal ground settlement was observed, influenced by the depth of the excavation and its aspect ratio. This research contributes to a better understanding of deformation in large-scale excavations.

Liang et al. [21] conducted a study detailing a large-scale basement excavation adjacent to a metro station, measuring 236.7 m in length, 145.8 m in width, and 23.2–27.3 m in depth, in soft clay. The excavation, divided into six zones by five partition walls, used a zoned-excavation approach to minimize impact on nearby metro and shield tunnels. Extensive monitoring covered lateral wall deflections, surface settlements, and vertical/horizontal displacements of the metro station and tunnels. Analysis revealed diaphragm walls moving towards the excavation, significant ground settlements, tunnel track heave within the station, and substantial shield tunnel settlements. Horizontal movements and elongations in the shield tunnel were also observed due to excavation-induced stress relief.

Ho and Gao [22] noted that their research case was located in Xizhi District, New Taipei City, Taiwan, with an excavation depth of 9.2 m and an area exceeding 2 hectares. The excavation was conducted without support, using diaphragm walls in conjunction with internal and external buttress walls of varying lengths. Additionally, a spanning floor slab around the perimeter was constructed using the top-down approach and also functioned as part of the retaining structure system. For geotechnical analysis, a three-dimensional numerical method (GTS) was employed to simulate and analyze the stability and deformation of the retaining walls. Besides the three-dimensional analysis, the case was also simplified for comparison using a one-dimensional method. Due to some uncertainties in the analysis results, emergency response plans were prepared in advance, allowing for immediate reinforcement if necessary. The actual deformation measured post-excavation was smaller than anticipated. This paper compares and analyzes the results with actual measurements, reviewing areas for improvement in the analysis process to serve as a reference for similar future cases.

This section's cases are summarized in Table 1 and compared large-scale deep excavation cases between Mainland China and Taiwan. Given that the majority of recent literature from Mainland China is based on studies of actual monitoring cases, subsequent discussions will primarily focus on two specific Taiwanese cases as the main points of reference for summarization.

Table 1. Large-scale deep excavation case comparison table.

Researcher	Location	Depth/Area	Numerical Analysis Method	Construction Method (Supported/Unsupported)	Field Monitoring	Key Findings
Liu et al. [18]	Shanghai/China	10.9–15.6 m/ 70,500 m ²	3D Numerical Method	Bottom-Up (Unsupported)	Wall Deflection, Ground Subsidence	Maximum wall deformation and ground subsidence exceed 0.86% of excavation depth
Liu et al. [19]	Shanghai/China	18.4 m/ approx. 10,000 m ²	No	Bottom-Up (Supported)	Wall Deflection, Vertical Wall and Column Movements, Ground Subsidence	Unique deformation characteristics due to the triangular shape of the pit
Ren et al. [20]	Chengdu/China	20 m/25,720 m ²	No	Bottom-Up Central-island (Supported)	Column Movements, Deflections, Internal Stress, Anchor Cable Forces, Ground Settlement, Water Levels	Maximum column deflection usually occurs at the top
Liang et al. [21]	Shanghai/China	23.2–27.3 m/ 31,309 m ²	Finite Element Method	Zoned Excavation (Unsupported)	Lateral Wall Deflections, Surface Settlements, Metro Station and Tunnels Vertical/Horizontal Displacements	Significant ground settlements and horizontal movements in metro station and tunnels
Ho and Gao [22]	Xizhi District, New Taipei City/Taiwan	9.2 m/over 2 hectares	GTS 3D Numerical Method	Peripheral Top-Down and Central Bottom-Up (Unsupported)	Wall Stability and Deformation	Actual deformation smaller than anticipated
This Study	Zhonghe District, New Taipei City/Taiwan	12.25 m/ 13,720 m ²	Plaxis 3D Finite Element Method	Peripheral Top-Down and Central Bottom-Up (Unsupported)	Lateral Displacement of Diaphragm Walls, Impact of Back-Pull Slabs and Cross Walls	Zoned excavation effectively controls lateral displacement on longer sides of the site

2. Materials and Methods

2.1. Research Methodology and Steps

This study utilizes real engineering case data and the finite element software PLAXIS 3D 2017 for its analysis. It involves a detailed comparison of field monitoring data with the results obtained from the analysis, thereby verifying the appropriateness of the chosen soil and structural parameters. Additionally, the study delves into the effects of zoned excavation, back-pull slabs, and cross walls on the deformation of retaining walls, using practical models for a more accurate representation.

The simulation process begins with the PLAXIS 3D 2017 software, tailored to the specific construction site conditions. This includes incorporating data from drilling reports, soil experimental parameters, and monitoring reports to set accurate parameters for the numerical simulation. The model is then constructed, taking into account the site's geometrical conditions and boundary settings. A key aspect of the simulation is its adherence to the actual construction conditions of the site. The simulation outcomes are then cross-referenced with on-site monitoring data, ensuring the validity of the soil and structural parameters used, as well as the construction steps simulated. These findings establish a baseline for the subsequent section, which focuses on analyzing the effectiveness of techniques like zoned excavation, the application of back-pull slabs, and the utilization of cross walls.

2.2. Case Introduction

This case study examines a construction project in the Zhonghe District of New Taipei City, featuring a notable 17-floor above-ground structure, standing 69.55 m tall, with three basement levels. Occupying a trapezoidal area of approximately 13,720 square meters, the site extends from 90.1 to 181.6 m east–west and 91.5 to 114.4 m north–south. It is encircled by various urban elements, including roads, an elevated MRT bridge, a gas station, metal buildings, and a seven-story building, as illustrated in Figure 6. The construction includes a 0.8 m thick diaphragm wall with depths ranging between 27 and 30 m. To control wall displacement, a “Peripheral Top-Down and Central Bottom-Up” method was employed, integrating cross walls, multiple buttress walls, and 0.4 m thick back-pull slabs. The excavation reached a depth of 12.25 m, supported by a raft foundation.

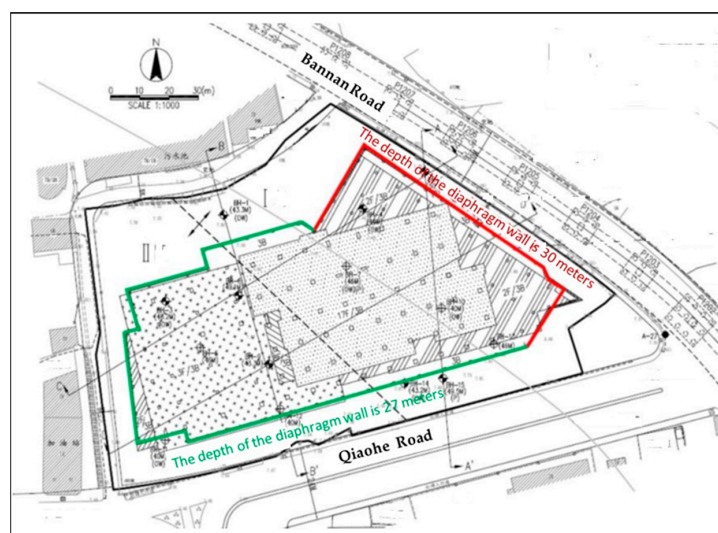


Figure 6. Site location map.

(1) Soil Layer Overview

Extensive data collection from 15 boreholes on-site, combined with laboratory test results and data from neighboring sites, led to the identification of around 13 distinct soil layers within a 50 m depth, as detailed in Appendix A, Figure A1. The borehole profiles,

along with the distribution depth, physical properties, and engineering characteristics of each soil layer, are elaborated in Table A1 and Supplementary Figures S1–S5.

(2) Diaphragm Wall Installation

In this engineering case study, the diaphragm walls were categorized into two depth groups: 30 m and 27 m, each with a thickness of 0.7 m. The project aimed to minimize wall deformation and its impact on adjacent structures during excavation. To achieve this, a combination of cross walls, internal buttress walls, and external buttress walls were strategically installed, as illustrated in Figure 7. The installation method for these structures mirrored that of the diaphragm walls.

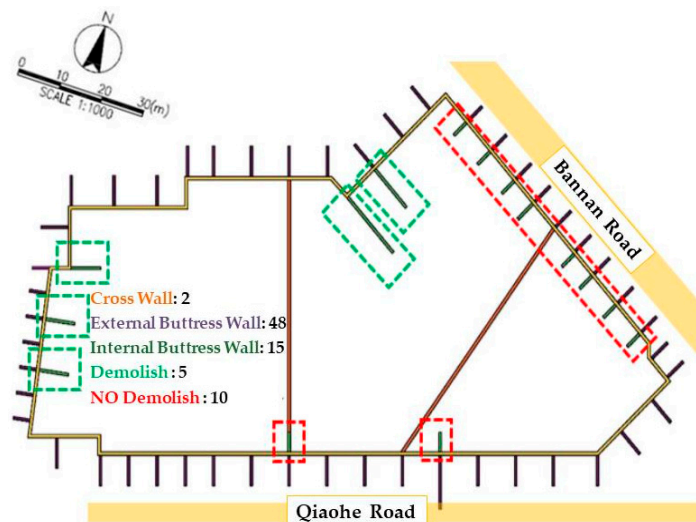


Figure 7. Plan layout of diaphragm wall, internal buttress wall, external buttress wall, and cross wall.

Specifically, two cross walls were erected; one intersected the diaphragm wall perpendicularly, while the other was positioned at a non-perpendicular angle. These walls, which extended approximately 60 m from a depth of GL -2.4 m to -25 m, were gradually removed as excavation progressed. The site also included fifteen internal buttress walls. Notably, eight of these walls near Banan Road and two near Qiaoh Road were not removed and later integrated into the final structure. In contrast, the remaining five internal buttress walls were removed during the excavation process. The depth of these internal and external buttress walls varied: the eight internal walls near the MRT on Banan Road extended from GL -2.4 m to -30 m, while the others ranged from GL -2.4 m to -27 m. An important aspect of this project was the joint connections between the diaphragm walls, cross walls, and both internal and external buttress walls, which were executed using T-shaped and cross-shaped joints to ensure structural integrity and stability.

(3) Monitoring System

Given the site's proximity to neighboring buildings, roads, and the MRT, rigorous construction control was essential. The primary goal of the monitoring system was to ensure the safety of the excavation work and the integrity of nearby structures. Monitoring included diaphragm wall deformation, groundwater level changes, and the settlement and tilting of neighboring buildings and roads. The monitoring equipment comprised internal and external wall inclinometers, strain gauges, water level observation wells, building tiltmeters, settlement observation points, and piezometers. This study particularly focused on inclinometer monitoring data to validate the numerical model's accuracy in comparison to the simulation results.

2.3. Numerical Simulation

PLAXIS, renowned for its proficiency in finite element analysis, particularly in geotechnical engineering, is increasingly favored in both academic and professional realms due

to its comprehensive features and user-friendly graphical interface. This research utilizes PLAXIS 3D 2017, and the following outlines the model establishment procedure for simulating deep excavation engineering using this software:

- (1) **Defining the Overall Model Boundary Profile:** The initial step involves calculating the dimensions of the construction site based on the area and excavation depth. For this model, the boundary extends 3 to 5 times the excavation depth from the diaphragm wall. Due to adjacent building loads, a fivefold extension is used in this case. Drilling reports inform the thickness and groundwater level of each soil layer, with additional consideration for irregular layers. The soil body's boundaries are defined with roller supports, allowing only vertical movement and hinge supports to limit both vertical and horizontal displacements. The bottom boundary is set at either a hard layer or a non-influential depth, using hinged nodes, while the side boundaries employ roller supports.
- (2) **Defining Soil Parameters:** Soil parameters for each layer are determined from drilling reports, indoor experiments, and empirical formulas. These parameters are then applied to the already drawn model, defining each soil layer's characteristics.
- (3) **Simulation of Deep Excavation Site:** The structures involved in deep excavation engineering—including diaphragm walls, cross walls, internal and external buttress walls, structural slabs, back-pull slabs, and foundation slabs—are simulated using plate elements. Geometric shapes are drawn and defined as plate elements, followed by applying material parameters to each structure.
- (4) **Simulation of Neighboring Building Loads:** Due to the absence of detailed construction data for neighboring buildings, the simulation uses plate and rigid body elements, with assumptions based on relevant literature and common engineering practices.
- (5) **Setting Construction Steps and Water Levels:** The construction process is set according to the actual steps taken on site. Water levels are adjusted around the excavation face to facilitate dry conditions for construction and ensure quality.
- (6) **Defining Grid and Grid Density:** Once the previous steps are complete, the grid is generated, with densification around the excavation face to enhance the accuracy of the analysis. This study opts for a medium grid density.
- (7) **Starting the Calculation:** With all parameters and configurations set, the final step is to initiate the calculation process in PLAXIS, leading to the analysis of the simulation results.

Based on the aforementioned model establishment procedure, the detailed content is as follows:

(1) Model Setup

This stage involves configuring the numerical model to mirror the actual case study. The model's excavation area and geometric shape are precisely aligned with the original site's size and geometry. The setup includes accurate depth settings for each stage of excavation, diaphragm walls, cross walls, internal and external buttress walls, internal structural slabs, and back-pull slabs, all of which are matched to the depths in the original construction. The model's boundary is defined with a horizontal distance of five times the excavation depth from the diaphragm wall. The vertical depth of the model is set to 50 m, resulting in an overall model size of 313 m × 222 m × 50 m.

(2) Selection of Soil Parameters

The soil in this deep excavation case study is categorized into 13 distinct layers, comprising 5 sandy soil layers, 7 clay soil layers, and a bottommost gravel layer (as detailed in Appendix A, Figure A1 and Table A1). The Mohr–Coulomb soil model is employed for the analysis. For sandy and gravel layers, a drained analysis approach is used, while clay layers are analyzed using an undrained approach. The Mohr–Coulomb model primarily involves four parameters: c , ψ , E , and ν . For drained analysis, the model requires the following: effective modulus of elasticity (E'), effective Poisson's ratio (ν'), effective angle of internal friction (ϕ'), and effective cohesion (c'). The undrained model used in the study is

Undrained C . The Undrained C model analysis requires the following: undrained modulus of elasticity (E_u), undrained Poisson's ratio (ν_u), and undrained shear strength (S_u).

A. Young's Modulus (E)

Due to the disturbance during soil sampling, the Young's Modulus (E) obtained from experiments cannot be directly used for analysis. Therefore, it is often estimated using empirical formulas in practice. Common methods for determining E include using the Standard Penetration Test ($SPT-N$) values for sandy soils and converting them using empirical formulas, and for soft clays, since their strength comes from undrained conditions (S_u), they are converted into E for soft clay using empirical relationships. According to Liao [23] in "Application of Empirical Soil Parameters in Numerical Analysis", the empirical formulas for laboratory values of E proposed by various scholars are used for estimation, as shown in Equations (6) and (7):

For clay, the Young's Modulus (E_u) is used as:

$$E_u = 800 S_u \quad (6)$$

where the value of S_u is obtained from indoor triaxial tests (UU).

For sandy soil, E' is used as:

$$E' = 2800 N \quad (7)$$

B. Poisson's Ratio (ν)

The recommended range of values for Poisson's ratio for different soils is referenced from Ou [24].

C. Wet Soil Unit Weight (γ_t), Effective Cohesion (c'), and Effective Friction Angle (ψ')

Values for wet soil unit weight, effective cohesion, and effective friction angle can be obtained through drilling reports and indoor experiments.

D. Interface Element Strength

The interaction between soil and structural elements involves a partial transmission of shear stress, modeled using interface elements that are divided into elastic and plastic stages. The elastic stage represents conditions of small strain, while the plastic stage accounts for larger sliding displacements. Interface elements employ a strength reduction factor (R_{inter}) in their calculations. A factor of 1 suggests complete shear stress transmission, but typically in geotechnical engineering, the interaction between soil and structures is weaker than the soil body itself. Hence, a reduction factor (R_{inter}) of less than 1 is often used, with the PLAXIS user manual recommending a setting of 2/3 for a more realistic approximation.

In summary, the relevant soil parameters are organized as shown in Tables 2 and 3.

Table 2. Undrained material parameters.

Depth (m)	γ (kN/m ³)	S_u (kN/m ²)	E_u (kN/m ²)	ν_u	R_{inter}
0~0.5	18.6	29.4	23,520	0.495	0.67
5.5~7.2	18.3	39.24	31,392	0.495	0.67
11.0~14.1	18.5	49.05	39,240	0.495	0.67
17.4~20.6	18.6	58.86	47,088	0.495	0.67
25.1~29.3	18.8	78.48	62,784	0.495	0.67
31.6~38.6	18.5	98.1	78,480	0.495	0.67
38.6~43.2	20.7	107.91	86,328	0.495	0.67

Reference Source: (E) from Liao [23]; (ν) from Ou [24]; Refer to the recommended values in the Plaxis 3D manual and consider local drilling data for the remaining parameters.

Table 3. Drained material parameters.

Depth (m)	γ (kN/m ³)	ϕ' (°)	E' (kN/m ²)	ν'	R_{inter}
7.2~11.0	19.5	30	21,924	0.2	0.67
14.1~17.4	18.5	32	34,104	0.2	0.67
20.6~25.1	19.4	32	36,540	0.2	0.67
29.3~31.6	18.9	32	38,976	0.2	0.67
43.2~44.8	19.7	33	56,028	0.2	0.67
44.8~50	21.6	40	121,800	0.2	0.67

Reference Source: (E') from Liao [23]; (ν') from Ou [24]; Refer to the recommended values in the Plaxis 3D manual and consider local drilling data for the remaining parameters.

(3) Structural Parameters

The diaphragm wall has a thickness of 0.7 m. The construction depth near the MRT side (Banan Road) is from GL -2.4 m to -30 m, with a penetration depth from GL -12.25 m to -30 m. On the non-MRT side, the construction depth is from GL -2.4 m to -27 m, with a penetration depth from GL -12.25 m to -27 m, as shown in Appendix A Figure A1. The internal and external buttress walls have the same construction depth as the diaphragm wall. To reduce deformation of the surrounding structures, 8 internal buttress walls near Banan Road and 2 near Qiaohe Road above the excavation face are not removed and will be considered as part of the structure in the future. All external buttress walls in this case are not removed. The cross wall has a thickness of 0.7 m, with a construction depth from GL -2.4 m to -25 m, and is removed stage by stage above the excavation face as the excavation depth increases. In this project, the joints between the diaphragm wall, cross wall, internal and external buttress walls are either T-shaped or cross-shaped.

The internal structural slab and back-pull slabs have a thickness of 0.4 m. The back-pull slabs is installed at GL -2.4 m and goes around the diaphragm wall of the site, as shown in Figure 8. It overlaps with the external buttress wall and diaphragm wall to enhance the overall stiffness of the diaphragm wall, reducing wall deformation. The top is then backfilled with soil. The internal structural slab is installed near the MRT side, as shown in Figure 8, located at GL -3.55 m. The diaphragm wall and internal buttress wall are set up with reserved reinforcement to connect with the internal structural slab, increasing the stiffness near the MRT side and reducing deformation in that area. The foundation slab has a thickness of 0.8 m and is placed at GL -12.25 m. Due to the large excavation area of this case, zoned excavation is used during construction. In areas where excavation is completed first, the foundation slab structure is implemented to enhance the stiffness of that area and reduce wall deformation.

The moduli of elasticity for the diaphragm wall, external buttress wall, non-removable internal buttress wall, and cross wall are calculated using the concrete's modulus of elasticity $E_c = 15,000 \times \sqrt{f'_c}$ (kgf/cm²), where f'_c is the 28-day compressive strength of concrete. For this study, f'_c is taken as 280 (kgf/cm²) for calculation. Parts of the internal buttress wall that need to be removed stage by stage will use low-strength backfill concrete, calculated with f'_c of 140 (kgf/cm²). Cross walls above the excavation face are removed as the excavation depth increases. To reduce costs, low-strength concrete with f'_c 140 (kgf/cm²) is used in the parent elements, and sandy soil is backfilled in the child elements, as shown in Figure 9. In numerical simulations, the removed part of the cross wall is simplified to low-strength concrete with $f'_c = 140$ (kgf/cm²). Table 4 lists the selected parameters for the diaphragm wall, internal buttress wall, external buttress wall, cross wall, back-pull slabs, internal structural slab, and foundation slab. Plaxis 3D uses a three-dimensional analysis approach, employing wall elements to simulate the diaphragm wall, buttress walls, and cross wall. It is assumed that the diaphragm wall, buttress walls, and cross wall are homogeneous and fully integrated, without considering poor construction conditions. Therefore, a linear state

is used, and $G_{12} = G_{13} = G_{23} = E_c / 2(1 + \nu_{12})$, where G is the shear modulus. Table 4 shows the parameters for the diaphragm wall, buttress walls, and cross wall.

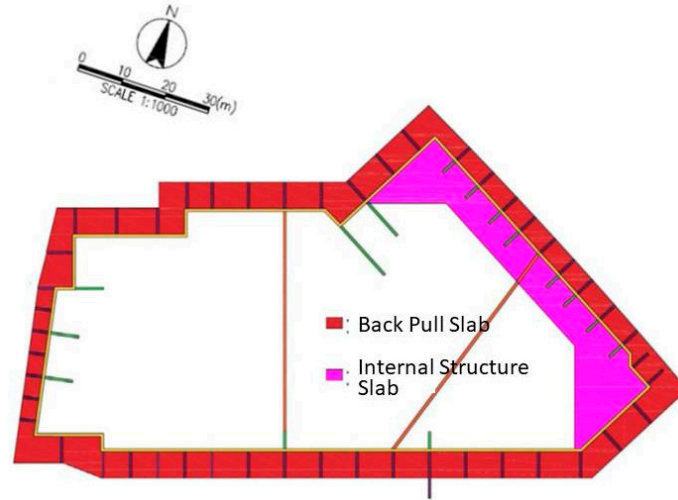


Figure 8. Location diagram of back-pull slab and internal structural slab.

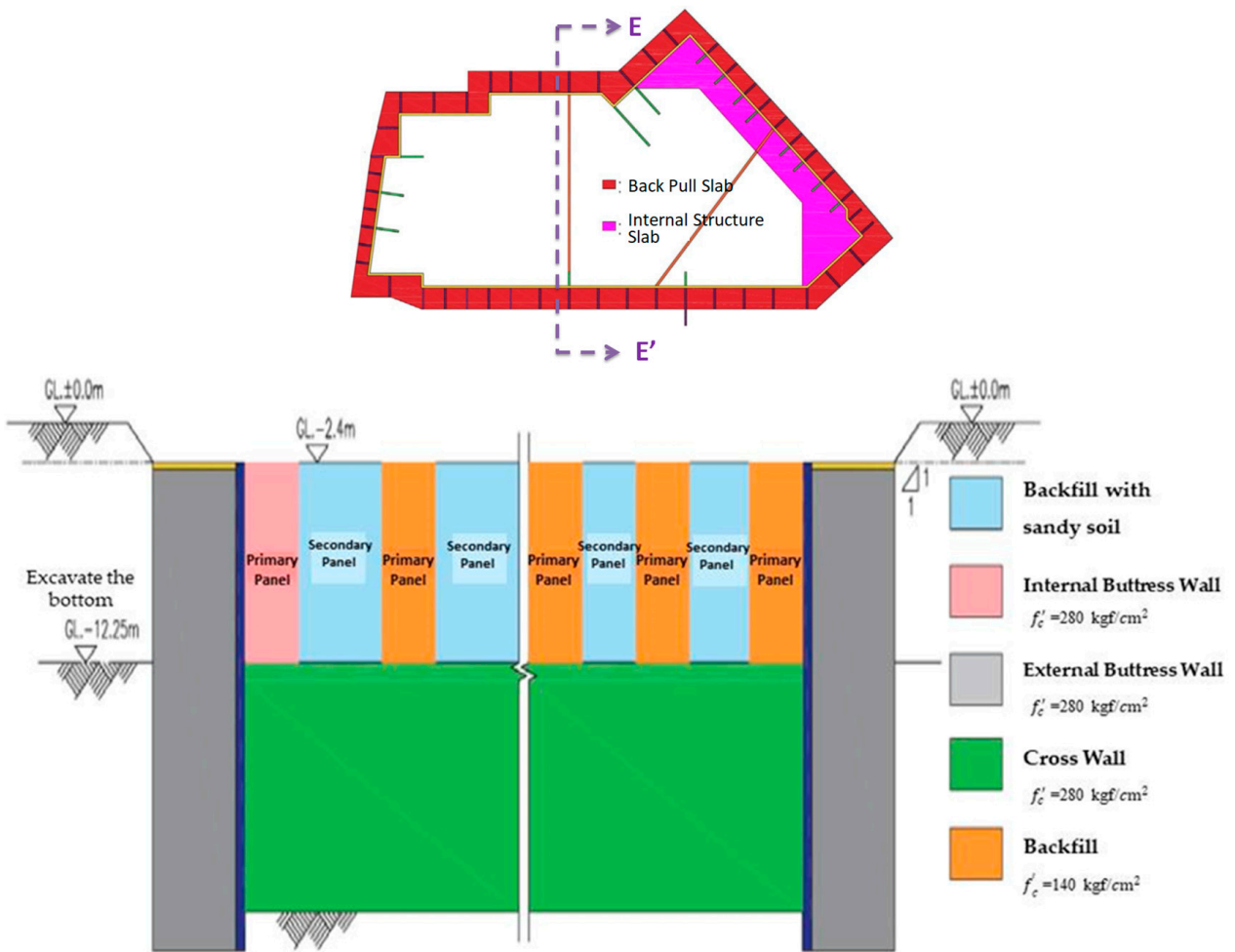


Figure 9. Cross-section diagram of excavation and cross wall.

Table 4. Structural parameters of diaphragm wall, buttress wall, cross wall, back-pull slabs, external structural slab, and foundation slab.

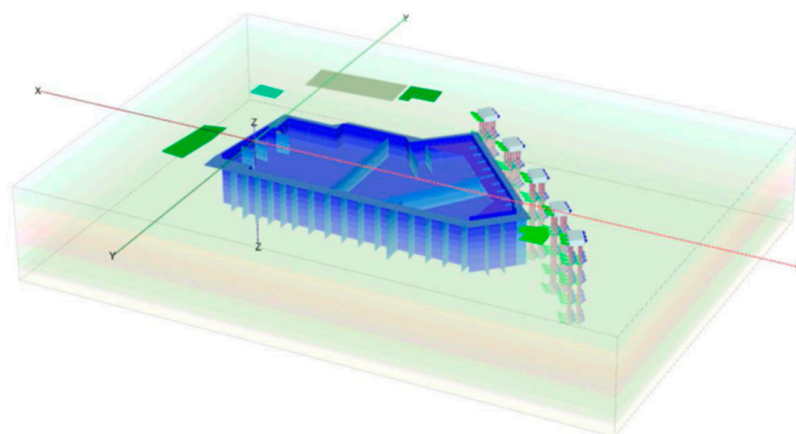
Type	Thickness (m)	Depth (m)	E (kN/m ²)	Poisson's Ratio ν	f'_c (kg/cm ²)
Diaphragm walls	0.7	2.4~27 2.4~30	2.42×10^7	0.15	280
Buttress walls (Layered Elimination)	0.7	2.4~12.25	1.74×10^7	0.15	140
Buttress walls	0.7/0.6	2.4~27 2.4~30	2.42×10^7	0.15	280
Cross walls (Layered Elimination)	0.7	2.4~12.25	1.74×10^7	0.15	140
Cross walls	0.7	12.25~27	2.42×10^7	0.15	280
1FL Back-Pull Slabs	0.4	2.0~2.4	2.42×10^7	0.15	280
B1F Internal Structure Slabs	0.4	3.55~3.95	3.02×10^7	0.15	420
Foundation Slab	0.8	11.45~12.25	2.42×10^7	0.15	280
Back-pull Slabs					

Data Source: Provided by the on-site construction team of Huida Construction for this case.

(4) Road and Nearby Structural Load Parameter Settings

In this case study, there are structures and roads surrounding the site. To closely simulate the actual conditions, the analysis considers the impact of structural load and road load on the excavation of the site. In previous studies, the simulation of structural and road loads was typically applied as surface loads on the ground, simplifying the analysis. The road and neighboring building loads remain active on the surface, representing conditions that already existed before the start of the project.

Based on common engineering experience, it is assumed that the load of one floor above ground is 1 t/m^2 ; the road load is also assumed to be 1 t/m^2 . For the concrete of the MRT pile cap structure on the road, the compressive strength f'_c is $280 \text{ (kgf/cm}^2\text{)}$, the thickness is 3 m , and the unit weight γ is $23.54 \text{ (kN/m}^3\text{)}$. The structural load values of neighboring buildings (1F to 3F and 7F) are, respectively, 9.81 , 19.62 , 29.43 , and 68.67 KN/m^2 . The structural model of the analysis is shown in Figure 10.

**Figure 10.** Structural model diagram.

(5) Zoned Excavation

Due to the large site area of $13,720 \text{ m}^2$ in this case study, it is necessary to conduct zoned excavation. Based on the construction conditions of the site, the daily excavation volume is approximately 1500 m^3 . After excavating each zone, foundation slab construction must be carried out, which typically takes about 7 days per zone. According to the site construction plan, the entire site is divided into 6 areas for zoned excavation, as shown in Figure 11. The excavation areas of each zone are detailed in Table 5.

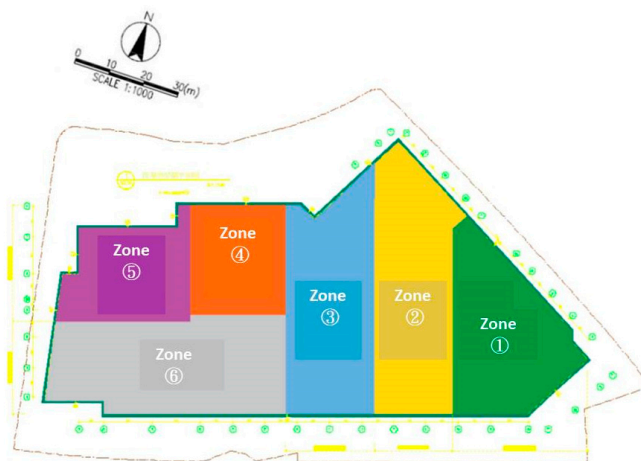


Figure 11. Zoned excavation area diagram.

Table 5. Area of zoned excavation.

Excavation Zone	Area	Location Photo
Zone ①	1307	Figure S6
Zone ②	1506	Figure S7
Zone ③	1500	Figure S8
Zone ④	822	Figure S9
Zone ⑤	884	Figure S10
Zone ⑥	1664	Figure S11
Total Area	7683	

2.4. Construction Steps

Finite element method analysis is used to simulate the construction steps, divided into 13 stages, to investigate the impact of the excavation process on lateral displacement changes. The aim is to find the optimal analysis method, aligning the simulation more closely with actual conditions. Due to the implementation of internal structural slabs in certain areas of this case, the construction steps are divided into the process shown in Figure 12.

During the analysis simulation, the construction process is divided into 13 steps:

- (1) Load neighboring buildings and roads, and calculate initial stress.
- (2) Excavate the entire site to (GL -2.4 m).
- (3) Install diaphragm walls, cross walls, internal buttress walls, and external buttress walls, and reset displacements to zero.
- (4) Construct external structural slab (GL -2.4 m), backfill certain areas.
- (5) Excavate areas with internal structural slabs to (GL -5.5 m), and lower the groundwater level to (GL -5.5 m).
- (6) Install internal structural slabs (GL -3.55 m).
- (7) Excavate the first zone to (GL -12.25 m), and lower the groundwater level to (GL -12.25 m).
- (8) Excavate the second zone to (GL -12.25 m), and install foundation slab for the first zone (GL -12.25 m).
- (9) Excavate the third zone to (GL -12.25 m), and install foundation slab for the second zone (GL -12.25 m).
- (10) Excavate the fourth zone to (GL -12.25 m), and install foundation slab for the third zone (GL -12.25 m).

- (11) Excavate the fifth zone to (GL -12.25 m), and install foundation slab for the fourth zone (GL -12.25 m).
- (12) Excavate the sixth zone to (GL -12.25 m), and install foundation slab for the fifth zone (GL -12.25 m).
- (13) Install foundation slab for the sixth zone (GL -12.25 m). Undrain (B) parameters.

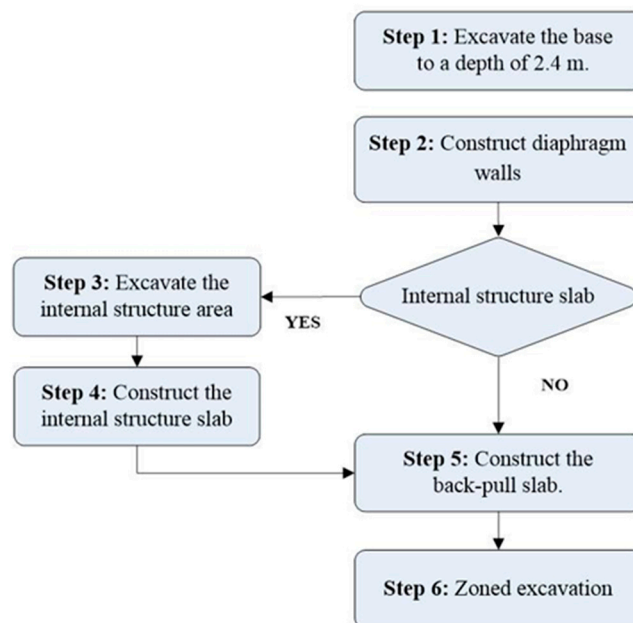


Figure 12. Process flow diagram of construction with and without internal structural slab.

2.5. Analysis Results and Case Verification

This section will discuss the comparison of the results from the finite element method software PLAXIS 3D for excavation engineering simulation analysis with the actual site monitoring data to verify the accuracy of the simulation. In this case, the site was monitored with 10 inclinometers to measure the lateral displacement of the diaphragm wall. The distribution map of the inclinometer monitoring locations is shown in Figure 13. This study focuses on verifying five inclinometers around the site, namely SIS02, SIS05, SIS06, SIS07, and SIS09. Figure 14a compares numerical analysis and monitoring data at the site's eastern monitoring point SIS02. At surface level GL -2.4 m, influenced by back-pull slabs, the analysis closely matches monitoring results. At excavation level GL -12.25 m, the monitored lateral displacement of the wall is 0.79 cm, while the simulation shows a slightly higher value of 0.4 cm. A 0.26 cm discrepancy is noted at the bottom of the diaphragm wall (GL -30 m) between internal and external inclinometers, indicating wall displacement. The simulation accounts for the back-pull slabs, non-removable internal and external buttress walls, and internal structural slab, which increase the wall's moment of inertia and stiffness, resulting in a cantilever deformation pattern.

Figure 14b shows that at the southern monitoring point SIS05, the numerical analysis matches the monitoring data, with cantilever-style deformation similar to that described by Wu et al. [25]. The lack of internal supports in this case study leads to slightly greater simulated lateral wall deformations compared to the monitored values, with the largest discrepancy being about 0.8 cm. The comparison at monitoring points SIS06 and SIS07 (Figure 14c,d) indicates similar trends in lateral wall displacement, with SIS06 showing less deformation due to its location between cross walls. The maximum displacement difference here is around 1.7 cm. At the northern monitoring point SIS10 (Figure 14e), the maximum error in lateral wall displacement is 0.3 cm above the excavation level, with a 0.73 cm difference observed at the wall bottom. The simulation shows increased wall stiffness near the corner due to back-pull slabs, leading to reduced displacement. The

maximum wall displacement in the simulation occurs at the excavation level, with a 0.3 cm difference from the monitored value.



Figure 13. Distribution map of inclinometer monitoring locations (where “SISXX” refers to monitoring point number XX).

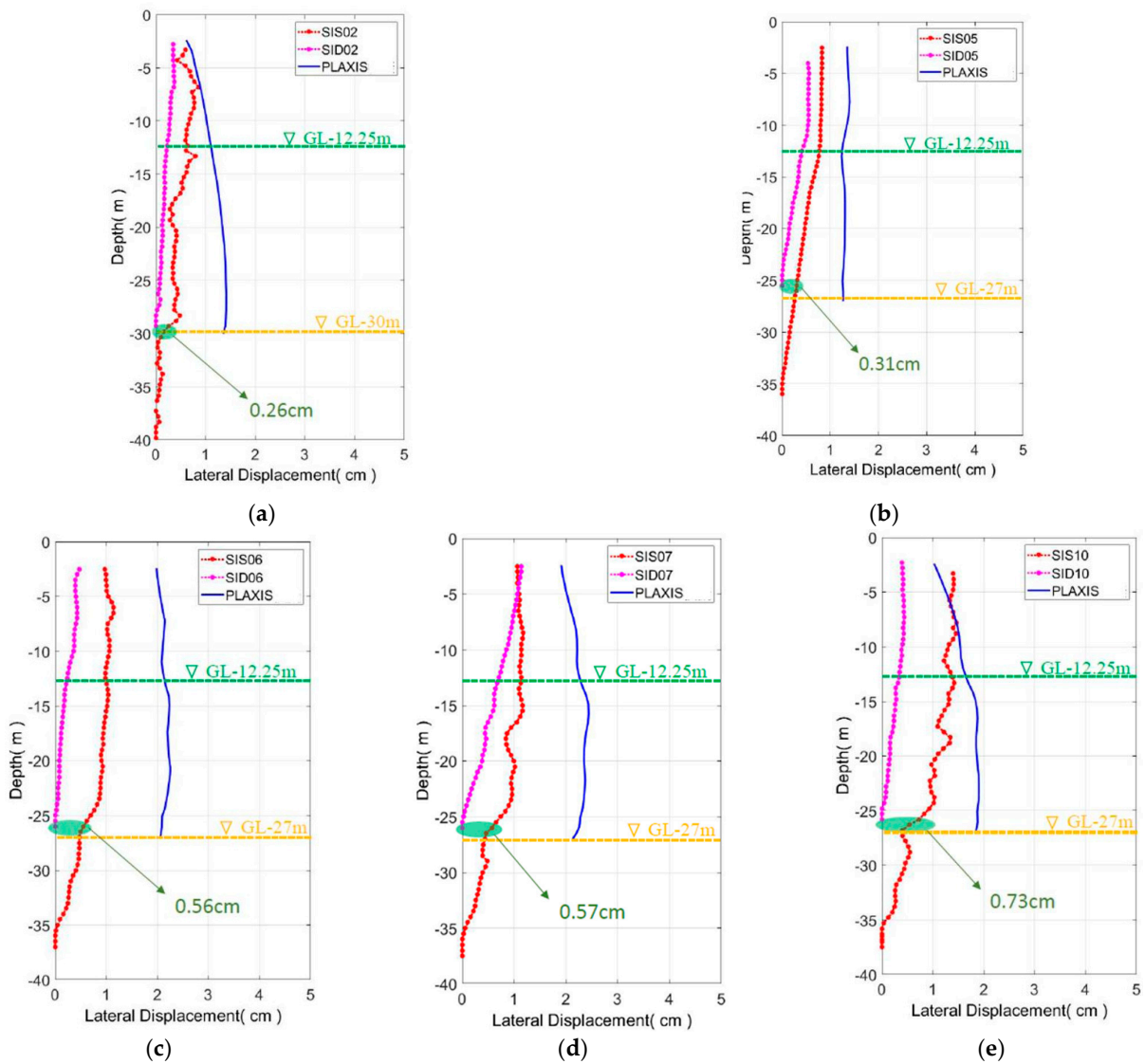


Figure 14. Comparison of numerical analysis results with monitoring values at each monitoring point: (a) SIS02; (b) SIS05; (c) SIS06; (d) SIS07; (e) SIS09.

The maximum lateral displacement (δ_{hm}) of the wall is compared. In this case, the data collected fall within the range of 0.2% to 0.5% of H_e (H_e being the final excavation depth), as outlined by Ou et al. [8] in their collection of research cases in the Taipei area. The maximum displacement of the wall in this study is on the lower end of the range proposed by Ou, as shown in Figure 15. This is likely due to the effects of zoned excavation and the implementation of the back-pull slabs, consequently reducing the overall lateral displacement of the wall.

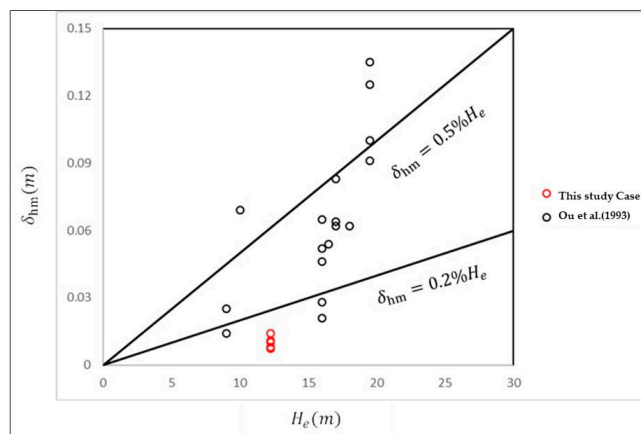


Figure 15. Relationship between maximum wall displacement and excavation depth [8].

From the comparison results, it is observed that the overall deformation trends of the diaphragm wall on the south side of the site in the analysis simulation are closer to the monitoring results. The wall deformation at the surface level GL -2.4 m in the simulation is generally lower. It is believed that the back-pull slabs can effectively suppress the lateral displacement of the diaphragm wall, primarily because the back-pull slab is implemented at the surface, enhancing the overall stiffness of the diaphragm wall at that location. To better understand whether the implementation of the back-pull slabs indeed effectively suppresses wall deformation, further discussion will follow in Section 3. Due to the large excavation area of this site, and the considerable length and width of the site without internal supports, a slight inward translation of the diaphragm wall body was observed in the numerical simulation. According to Ou [3], in unsupported excavation cases in soft soil, a toe translation phenomenon is also observed on the longitudinal side of the excavation. To better align with the actual construction process on-site, the simulation of construction procedures also adopts the same zoned excavation model as used on-site. Whether this directly affects the overall lateral displacement of the wall will be discussed in the next section.

2.6. Limitations and Impacts of the Plaxis 3D Model

PLAXIS, a finite element software for geotechnical and soil–structure interaction analysis, presents several limitations despite its robustness and versatility. These constraints are mainly in the following areas:

- **Element Number:** PLAXIS has a maximum limit on elements, which could restrict modeling in complex or large-scale projects, and more elements lead to increased computation time and resource usage.
- **Material Properties:** The software may not always accurately model the properties of heterogeneous soils or complex materials, and handling non-linear materials can present challenges.
- **Boundary Conditions:** Although PLAXIS offers various options for boundary conditions, it might fall short in specialized or extreme cases, and replicating real-world conditions accurately can be difficult.

- Loading Conditions: Simulating certain dynamic or cyclic loads, as well as extreme load scenarios, might exceed PLAXIS's capabilities.
- Analysis Types: The software has limitations in long-term consolidation and creep analysis, as well as simulating certain environmental effects.
- Software and Hardware Interaction: The performance of PLAXIS is hardware-dependent, and there may be constraints in parallel processing efficiency for large or complex models.

Engineers and researchers using PLAXIS should be aware of these limitations and consider supplementing their work with other tools, tests, or models to achieve comprehensive and accurate outcomes. It is also important to regularly consult PLAXIS's latest manuals and technical documents for updated information on its capabilities and limitations.

3. Case Study

This section aims to explore three major aspects related to the case study: the impacts of zoned excavation, back-pull slabs, and cross walls on the lateral displacement of diaphragm walls. Individual benefit analyses will be conducted to examine the effectiveness of these methods. The goal is to determine if they can effectively suppress the lateral deformation of diaphragm walls, thereby indirectly reducing the impact on neighboring structures and ensuring the safety of the site to prevent engineering disasters. The research in this section is based on the model, soil layers, and retaining structure parameters established in the previous sections.

This study uses an evaluation metric for wall displacement, adopting the maximum deflection ratio (MDR), as proposed by Lim et al. [16], to assess the impact of wall deformation, as shown in Equation (1).

3.1. Impact of Excavation

This section explores the impact of changing the excavation area on the lateral deformation of diaphragm walls. Using the model from the original engineering case, which involved excavation in six zones, this study investigates the effects of simplified excavation methods: three-zone excavation and layer-by-layer excavation. The analysis focuses on the longitudinal displacement of the diaphragm walls.

(1) Impact of Zoned Excavation

In the original case, the entire site was divided into six zones for excavation, as shown in Figure 11. To examine the effect of zoned excavation on diaphragm walls, the excavation zones were simplified by dividing the site into three zones based on the placement of cross walls, as illustrated in Figure 16. The respective areas of excavation zones 1 to 3 are 1487, 3089, and 3107 m², with the total area being 7683 m². The study focuses on two cross-sections: the ground surface at GL −2.4 m and the excavation face at GL −12.25 m. Lateral displacement of the diaphragm walls for these two sections is depicted in Figure 17.

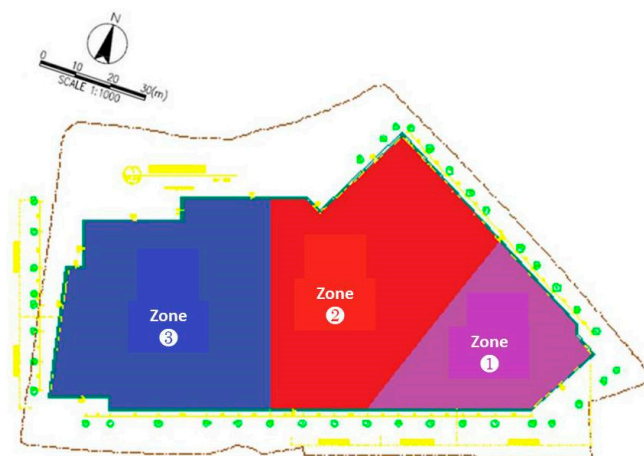


Figure 16. Simplified zoned excavation Areas.

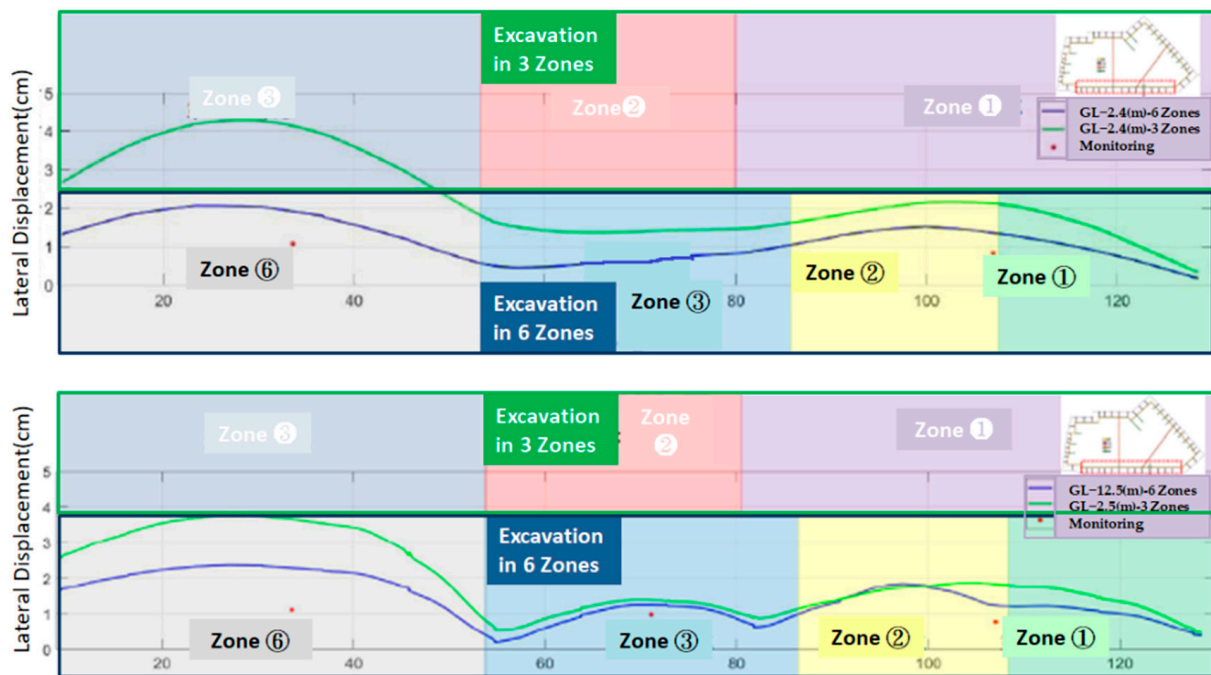


Figure 17. Lateral displacement diagrams of the diaphragm wall at GL -2.4 m and -12.25 m.

Based on the effect of corner arching, the maximum lateral displacement of the diaphragm wall occurs in the longitudinal direction. In this case, the longest segment of the diaphragm wall is located near the bridge and road, with a length of 118.30 m. Therefore, the analysis and comparison are focused on the wall in this area.

For two different zoned excavations with excavation sequences as shown in Figures 11 and 16, both progress from right to left in the diagrams. The impact of different zoned excavations on the maximum deformation of the diaphragm wall is summarized in Table 6. It is observed that dividing the zoned excavation into six zones results in a smaller maximum wall displacement than that of three-zone excavation. In both types of zoned excavation, when the length of the first excavation zone is 21.39 m, the lateral displacement of the wall at GL -2.4 m is 1.33 cm. When the length increases to 46 m, the lateral displacement of the wall increases to 2.09 cm, a significant increase of 0.75 cm. The six-zone excavation simulation, located at the GL -12.25 m excavation face, shows that the first and second excavation zones have a mitigating effect on wall deformation, as clearly seen in Figure 17. The third excavation zone of the six-zone excavation has the same length as the second excavation zone of the three-zone excavation (27 m). The lateral displacement of the wall is 1.51 cm and 1.63 cm, respectively, with no significant increase in wall lateral displacement. The slight increase in displacement is mainly influenced by the previous excavation zone. Finally, comparing the sixth excavation zone of the six-zone excavation with the third excavation zone of the three-zone excavation, both have excavation ranges of 44.95 m. The maximum lateral displacement of the wall at GL -2.4 m is 2.06 cm and 4.28 cm, respectively, showing that this zone significantly suppresses wall deformation, with a difference of 2.22 cm. In summary, zoned excavation, in the absence of internal support, has a significant effect on suppressing lateral deformation of the diaphragm wall, enhancing overall construction safety, and indirectly reducing its impact on surrounding structures.

(2) The impact of excavation by layers:

The original case study divided the site into six areas for excavation to explore the impact of sectional excavation on the lateral displacement of the diaphragm wall. For analysis, the excavation area was simplified, using layer-by-layer excavation. This study utilizes the model from the original engineering case, which involved sectional excavation in six areas. In this study, layer-by-layer excavation was employed, divided into four stages.

The study focuses on two cross-sections: the ground surface after excavation at GL -2.4 m and the excavation face at GL -12.25 m. The lateral displacement of the diaphragm wall is illustrated in Figure 18 (top and middle diagrams).

Table 6. Maximum wall displacement in zoned excavation at GL -2.4 m.

Zone	Max. Displacement in 6 Zones (cm)	Max. Displacement in 3 Zones (cm)	Max. Displacement in 6 Zones (cm)	Max. Displacement in 3 Zones (cm)
	Local @ GL -2.4 m		Local @ GL -12.25 m	
Zone 1	1.33	2.09	1.22	1.87
Zone 2	1.51	1.63	1.84	1.23
Zone 3	1.08	4.28	1.12	3.77
Zone 6	2.06	-	2.37	-

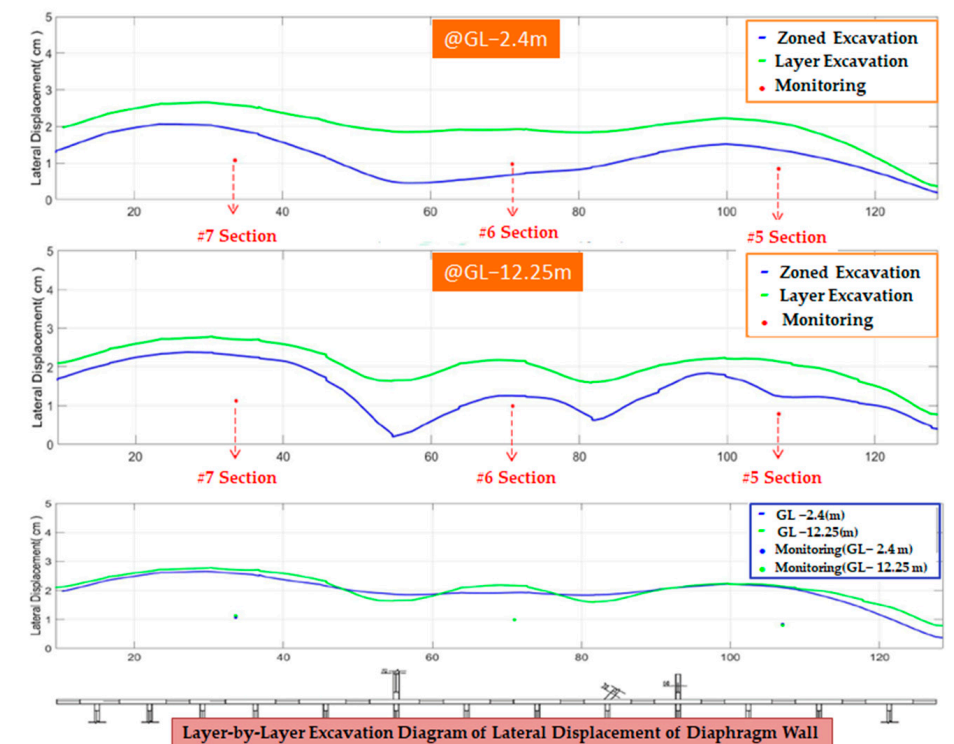


Figure 18. Comparative diagram of lateral displacement of diaphragm wall in zoned excavation and layer-by-layer excavation.

By comparing the lateral displacement of the diaphragm wall in sectional excavation with layer-by-layer excavation from the previous section, analysis is conducted on three cross-sections. At the ground surface GL -2.4 m, the lateral displacement values of the diaphragm wall in all three cross-sections are greater in layer-by-layer excavation compared to sectional excavation, as shown in Table 7. The differences at the three cross-sections are 0.67 cm, 1.25 cm, and 0.74 cm, respectively. Similarly, at the final excavation face GL -12.25 m, the lateral displacement values in layer-by-layer excavation exceed those in sectional excavation, with differences of 0.41 cm, 0.91 cm, and 0.9 cm at the three cross-sections. In Figure 18 (bottom diagram), it is evident that the excavation values at the ground surface and the deformation trends at the final excavation face are very similar in layer-by-layer excavation.

Table 7. Comparison of displacements in sectional excavation and layer-by-layer excavation.

Zone	Zoned Exc.	Layer Exc.	Zoned Exc.	Layer Exc.
	Displacement (cm)			
	Local @ GL −2.4 m		Local @ GL −12.25 m	
#5 Section	1.91	2.58	2.29	2.7
#6 Section	0.67	1.92	1.25	2.16
#7 Section	1.33	2.07	1.22	2.12

From the above data, a conclusion can be drawn: in large-scale deep excavations, dividing the site into several independent small excavation areas can effectively suppress the lateral displacement of the main diaphragm wall. This construction method can effectively protect surrounding facilities. In this study's case, the maximum displacement of the wall is located in the lower half of the range proposed by Ou [8]. The maximum lateral displacement of the wall, measured as δ_{hm} , is within 0.2% of H_e .

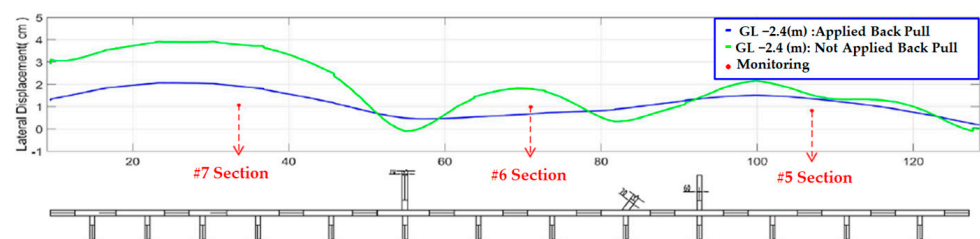
3.2. Effectiveness of Back-Pull Slabs

This section explores the impact of back-pull slabs on reducing the lateral deformation of continuous walls. The study uses the model from the original engineering case and analyzes two scenarios: with and without back-pull slabs. The analysis focuses on the site's lengthwise side, where the lateral displacement of the continuous wall is greatest. Comparisons are made at cross-sections 5, 6, and 7, where monitoring instruments are located. The maximum deflection ratio (MDR) is used to assess wall deformation, as shown in Equation (1).

The study, detailed in Table 8 and Figures 19–21 shows that back-pull slabs significantly reduce the lateral displacement of diaphragm walls, especially at cross-sections 6 and 7. With the slab, displacement at cross-section 6 is 0.63 cm compared to 1.81 cm without, and at cross-section 7, it is 1.91 cm versus 3.77 cm. The effect is weaker at cross-section 5 due to interactions between corner effects, sectional excavation, and cross walls. The slabs, installed at GL −2.4 m, increase wall stiffness and effectively control deformation. Without the slabs, walls experience greater inward displacement due to the lack of internal supports. This indicates that in unsupported conditions, back-pull slabs are effective in reducing lateral wall displacement.

Table 8. Wall displacement with and without back-pull slab.

Section	Wall Displacement (cm) with Back-Pull Slab	Wall Displacement (cm) without Back-Pull Slab	MDR (%)
#5 Section	1.33	1.46	8.9
#6 Section	0.63	1.81	65.2
#7 Section	1.91	3.77	49.3

**Figure 19.** Graph of wall displacement with and without back-pull slab.

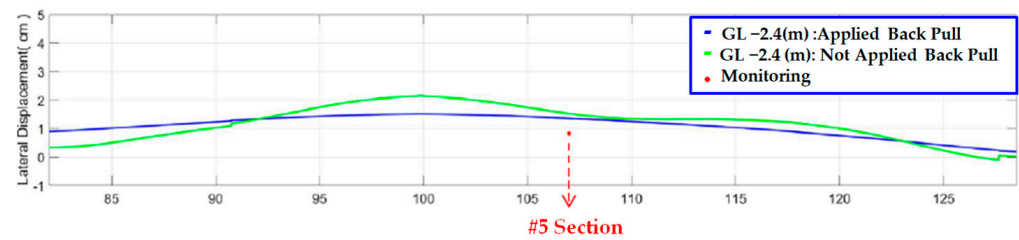


Figure 20. Graph of wall displacement at cross-section #5 with and without back-pull slab.

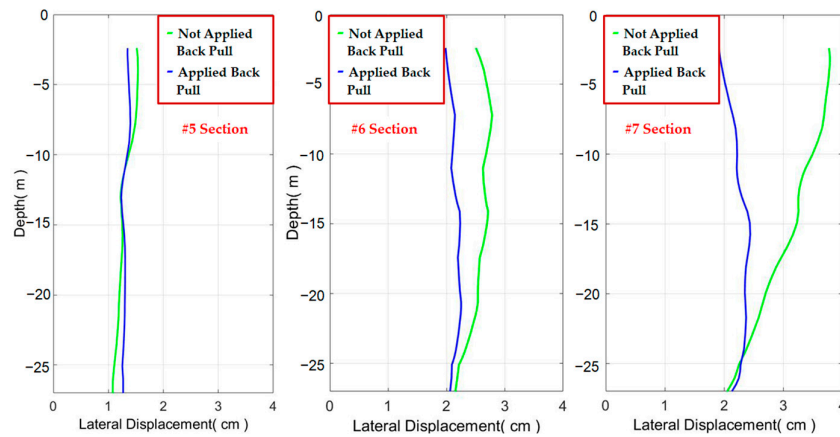


Figure 21. Lateral displacement graph of the wall at cross-sections #5 to #7.

3.3. The Effectiveness of Cross Wall Construction

This section evaluates the impact of cross walls on reducing lateral deformation of diaphragm walls in a large excavation site, as depicted in Figure 8. The study focuses on a 118 m segment along the bridge and road, assessing areas with cross walls both perpendicular and non-perpendicular to the diaphragm wall.

Figure 22 highlights the effect of cross walls on diaphragm wall stability. Figure 23 illustrates this in three areas (A, B, C), showing reduced wall displacement at cross wall locations. In Area A, the maximum deformation at GL -12.25 m reduces from 2.37 cm to 0.19 cm near the cross wall; at GL -2.4 m, it decreases from 2.05 cm to 0.49 cm. In Area B, deformation at GL -12.25 m drops from 1.25 cm to as low as 0.19 cm, and at the surface, from 0.89 cm to 0.45 cm. Area C shows similar trends, with maximum displacement decreasing from 1.84 cm to 0.63 cm and 0.38 cm at various points.

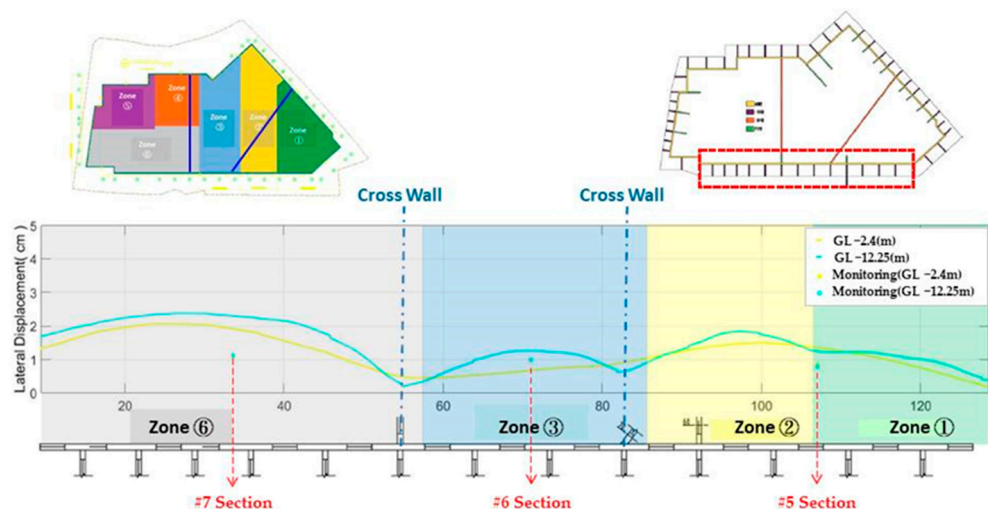


Figure 22. Lateral displacement graph of the diaphragm wall.

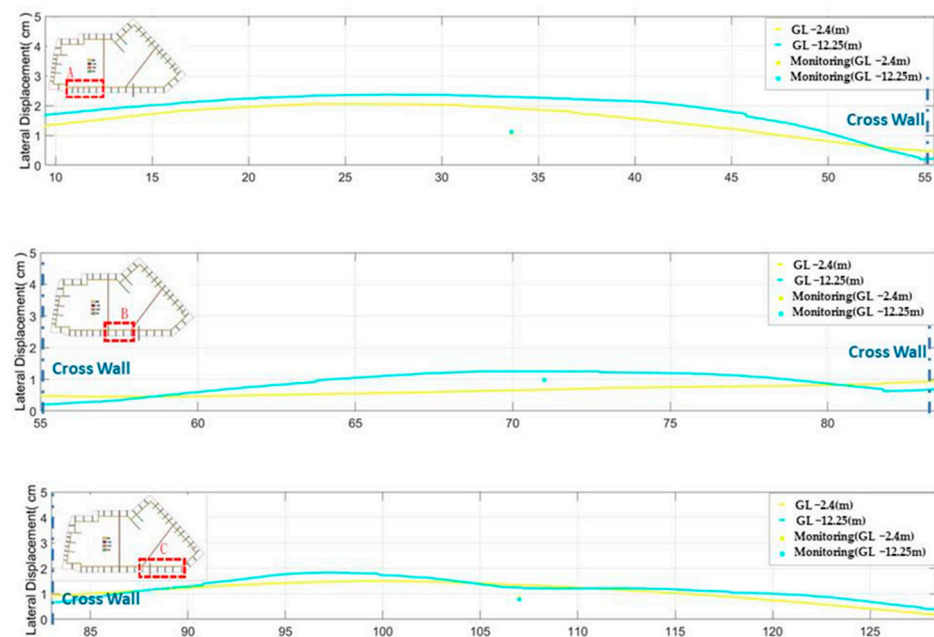


Figure 23. Lateral deformation graphs of the diaphragm wall in Areas A, B, and C.

The study confirms that cross walls, especially when perpendicular to diaphragm walls, significantly limit lateral displacement. This is quantified in Table 9, where perpendicular cross walls demonstrate greater deformation control. The analysis suggests that future designs should ideally align cross walls perpendicular to diaphragm walls for optimal deformation control.

Table 9. Benefits of perpendicular and non-perpendicular cross walls.

Level	Perpendicular Cross Wall Displacement (cm)	Non-Perpendicular Cross Wall Displacement (cm)
Surface Level (GL −2.4 m)	0.49	0.89
Final Excavation Level (GL −12.25 m)	0.19	0.63

4. Conclusions

This study utilizes PLAXIS 3D 2017 as a research tool, simulating a real-world excavation project for validation. By approximating the construction site conditions with the site's geometry, soil and structural parameters, and construction steps, and comparing these simulations with on-site monitoring results, the study verifies the model's credibility. Based on this model, further analyses were conducted to assess the impact of excavation methods, back-pull slabs, and cross walls on diaphragm wall displacement, aiming to explore effective ways to control deformation in large-scale deep excavations. The numerical analysis simulations are intended to provide references for both academia and the engineering field. The following are the conclusions and recommendations from this study.

4.1. Summary

- Impact of Excavation Methods on Lateral Displacement of Diaphragm Walls in Large Unsupported Deep Excavations:
 - Sectional excavation significantly reduces wall deformation. Designing smaller excavation areas in accordance with on-site construction can markedly lower lateral deformation.
 - Layer-by-layer excavation in this method shows less significant reduction in lateral wall deformation.

- Numerical simulations and monitoring data indicate that this construction method results in a cantilever-type wall deformation.
2. Lateral Displacement Phenomena of Diaphragm Walls:
 - The construction method in this study causes displacement at the toe of the diaphragm wall, as observed through external and internal inclinometers.
 - Different inclinometer installation depths may alter the assumed position of the neutral point. Both numerical analysis and monitoring show toe displacement, so there remains some discrepancy in accurately estimating lateral displacement through either method.
 3. Influence of Back-Pull Slabs on Lateral Wall Displacement:
 - In the construction method involving peripheral top-down and central bottom-up approaches, the study finds that back-pull slabs, when feasible in large site areas, significantly enhance the stiffness and connection between the main diaphragm wall and external buttress walls, effectively reducing lateral displacement. In this case, it could reduce up to 65.19% of the lateral deformation.
 4. Influence of Cross Walls on Lateral Wall Displacement:
 - Due to the large excavation area and elongated site width, this study analyzes the effect of two cross walls on wall displacement. Results show that even with a width of 60 m, cross walls can effectively control lateral displacement of the main diaphragm wall.
 - One of the cross walls, due to the site's shape, is not perpendicular to the diaphragm wall and shows less effective deformation control compared to perpendicular walls.
 - Horizontal steel stress meters in cross walls and inclinometer installation positions do not directly prove the mechanical behavior of cross walls; their effectiveness is primarily observed through numerical simulation.

This study significantly impacts large unsupported deep excavations, offering key insights into design and construction. It demonstrates that sectional excavation effectively reduces wall deformation, providing a critical reference for future projects. The research also highlights the importance of understanding lateral displacement in diaphragm walls, as observed through inclinometer data, enhancing predictive accuracy and design safety. Additionally, it reveals the effectiveness of back-pull slabs in increasing wall stiffness and connectivity, reducing lateral displacement. The analysis of cross walls' influence, particularly in wide excavations, further informs deformation control strategies. Overall, this study provides essential guidance for the design and execution of similar constructions, emphasizing innovative methods like back-pull slabs and cross walls for effective deformation management.

Based on the findings of this study, there are several significant applications in practical engineering contexts. The demonstrated effectiveness of sectional excavation in reducing wall deformation provides a valuable strategy for managing lateral displacement in large unsupported deep excavations. This approach can be particularly beneficial in urban areas where space constraints and the proximity of existing structures demand precise control of excavation impacts.

The study suggests that layer-by-layer excavation is a tailored solution for certain projects and that numerical simulations are key in designing against wall deformation. It also finds that back-pull slabs improve structural stability in large excavations, providing a cost-effective alternative to traditional supports. Furthermore, cross walls prove effective for lateral support across various excavation widths and shapes. Collectively, these insights inform better practices for deep excavation, enhancing safety and efficiency.

4.2. Recommendations

1. The biggest challenge in this study was model construction. The case is extremely complex, including diaphragm walls, cross walls, internal and external buttress walls, back-pull slabs, and internal structural slabs, combined with the site's irregular geometry, multiple turns, and sloping edges. This complexity often led to meshing failures at interfaces, requiring adjustments in overall mesh density and fine-tuning of conflicting structural coordinates to avoid small area mesh generation and model failures.
2. In Taiwan, engineering cases using this excavation method are currently very rare, which limits the scope of research findings. In the future, collecting and analyzing more cases related to this method could help in substantiating the research with additional relevant data.
3. For future monitoring device setup, placing inclinometers at the junctions of cross walls and diaphragm walls could allow for directly observing the impact of cross walls on diaphragm walls, facilitating validation with numerical simulations. Steel stress meters in cross walls should be installed on both sides of the wall to explore the force behavior of cross walls.
4. The analysis could be further enhanced by using a wider variety of soil models. Comparing a hardening soil model or hardening soil with a small strain model could identify the most conservative design approach, thereby increasing overall safety.

Supplementary Materials: The following supporting information can be downloaded at: <https://www.mdpi.com/article/10.3390/buildings14010023/s1>, Figure S1: Location Map of Borehole Profiles on the Site; Figure S2: Columnar Section Diagram of Borehole A A'; Figure S3: Columnar Section Diagram of Borehole B B'; Figure S4: Columnar Section Diagram of Borehole C C'; Figure S5: Columnar Section Diagram of Borehole D D'; Figure S6: Construction Status Map of Zone 1; Figure S7: Construction Status Map of Zone 2; Figure S8: Construction Status Map of Zone 3; Figure S9: Construction Status Map of Zone 4; Figure S10: Construction Status Map of Zone 5; Figure S11: Construction Status Map of Zone 6.

Author Contributions: Conceptualization, H.-W.C., C.-F.H., F.-H.T. and S.-L.C.; methodology, H.-W.C., F.-H.T. and S.-L.C.; formal analysis, H.-W.C. and F.-H.T.; investigation, F.-H.T.; writing—original draft preparation, F.-H.T. and C.-F.H.; writing—review and editing, C.-F.H. All authors have read and agreed to the published version of the manuscript.

Funding: This research was funded by the Ministry of Science and Technology, Taiwan, under contract No. NSTC 112-2221-E-027-047.

Data Availability Statement: The data presented in this study are available in supplementary material.

Conflicts of Interest: Author Fu-Huan Tsai was employed by the company Huaku Development Co., Ltd. The remaining authors declare that the research was conducted in the absence of any commercial or financial relationships that could be construed as a potential conflict of interest.

Appendix A

Table A1. Simplified soil layer parameter chart (provided by drilling report).

Soil Layer	Average Depth	γ_t (kN/m ³)	N	S_u (kN/m ²)	e	C'_{ref} (kN/m ²)	ϕ' (°)
CL1	0~−5.5	18.6	6	29.4	0.92	0.2	28
CL/ML1	−5.5~−7.2	18.3	3	39.24	1.00	0.2	27
SM1	−7.2~−11.0	19.5	9	—	0.65	0.2	30
CL/ML2	−11.0~−14.1	18.5	7	49.05	0.87	0.2	28
SM2	−14.1~−17.4	19.1	14	—	0.71	0.2	32
CL2	−17.4~−20.6	18.6	7	58.86	0.85	0.2	28
SM3	−20.6~−25.1	19.4	15	—	0.60	0.2	32

Table A1. Cont.

Soil Layer	Average Depth	γ_t (kN/m ³)	N	S_u (kN/m ²)	e	C'_{ref} (kN/m ²)	ϕ' (°)
CL3	−25.1~−29.3	18.8	7	78.48	0.79	0.2	29
SM4	−29.3~−31.6	18.9	16	—	0.76	0.2	32
CL-ML	−31.6~−38.6	18.5	10	98.10	0.90	0.2	30
CL4	−38.6~−43.2	20.7	22	107.91	0.55	0.2	32
SM5	−43.2~−44.8	19.7	23	—	0.60	0.2	33
GW/GP	−44.8 down	21.6	50	—	—	0.2	40

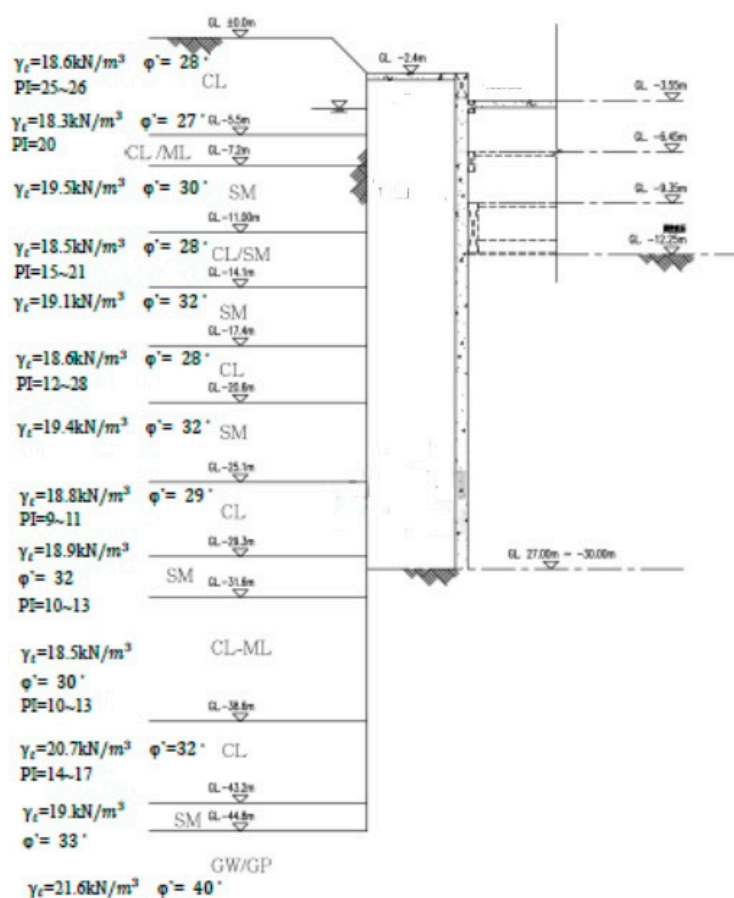


Figure A1. Excavation and underground cross-section diagram.

References

- Weidong, L.G.W. *Foundation Pit Engineering Handbook*, 2nd ed.; China Architecture & Building Press: Beijing, China, 2009.
- Lim, A.; Ou, C.-Y. Case Record of a Strut-free Excavation with Buttress Walls in Soft Soil. In *Proceedings of the 2nd International Symposium on Asia Urban GeoEngineering*; Springer Singapore: Singapore, 2018.
- Ou, C.Y. *Advanced Deep Excavation Engineering Analysis and Design*; Tech Books Incorporated: Taipei, Taiwan, 2017.
- Jeng, C.-J.; Ho, S.-K. A Case Study of 3-D Numerical Analysis for Nonstrut Construction Method in Huge Area Foundation Excavation. *J. Art Des. Huafan Univ.* **2016**, *11*, 75–87.
- Li, M.-G.; Zhang, Z.-J.; Chen, J.-J.; Wang, J.-H.; Xu, A.-J. Zoned and staged construction of an underground complex in Shanghai soft clay. *Tunn. Undergr. Space Technol.* **2017**, *67*, 187–200. [[CrossRef](#)]
- Wang, J.H.; Xu, Z.H.; Wang, W.D. Wall and Ground Movements due to Deep Excavations in Shanghai Soft Soils. *J. Geotech. Geoenviron. Eng.* **2010**, *136*, 985–994. [[CrossRef](#)]
- Clough, G.W.; O'Rourke, T.D. *Construction-Induced Movements of In Situ Wall, Design and Performance of Earth Retaining Structure*; ASCE: Reston, VA, USA, 1990.
- Ou, C.-Y.; Hsieh, P.-G.; Chiou, D.-C. Characteristics of ground surface settlement during excavation. *Can. Geotech. J.* **1993**, *30*, 758–767. [[CrossRef](#)]

9. Mana, A.I.; Clough, G.W. Prediction of movements for braced cuts in clay. *J. Geotech. Eng. Div.* **1981**, *107*, 759–777. [[CrossRef](#)]
10. Masuda, T.; Einstein, H.H.; Mitachi, T. Prediction of lateral deflection of diaphragm wall in deep excavations. *Doboku Gakkai Ronbunshu* **1994**, *1994*, 19–29. [[CrossRef](#)] [[PubMed](#)]
11. Wu, S.-H.; Ching, J.; Ou, C.-Y. Predicting wall displacements for excavations with cross walls in soft clay. *J. Geotech. Geoenviron. Eng.* **2013**, *139*, 914–927. [[CrossRef](#)]
12. Do, T.-N.; Ou, C.-Y.; Lim, A. Evaluation of factors of safety against basal heave for deep excavations in soft clay using the finite-element method. *J. Geotech. Geoenviron. Eng.* **2013**, *139*, 2125–2135. [[CrossRef](#)]
13. Chheng, C.; Likitlersuang, S. Underground excavation behaviour in Bangkok using three-dimensional finite element method. *Comput. Geotech.* **2018**, *95*, 68–81. [[CrossRef](#)]
14. Chen, S.-L.; Ho, C.-T.; Li, C.-D.; Gui, M.-W. Efficiency of buttress walls in deep excavations. *J. Geoeng.* **2011**, *6*, 145–156.
15. Hsiung, B.-C.; Yang, K.-H.; Aila, W.; Ge, L. Evaluation of the wall deflections of a deep excavation in Central Jakarta using three-dimensional modeling. *Tunn. Undergr. Space Technol.* **2018**, *72*, 84–96. [[CrossRef](#)]
16. Lim, A.; Hsieh, P.-G.; Ou, C.-Y. Evaluation of buttress wall shapes to limit movements induced by deep excavation. *Comput. Geotech.* **2016**, *78*, 155–170. [[CrossRef](#)]
17. Chuah, S.; Harry, S.T. Numerical study on a new strut-free counterfort embedded wall in Singapore. In Proceedings of the Earth Retention Conference 3, Bellevue, Washington, 1–4 August 2010.
18. Liu, G.; Guo, J.; Li, M.; Qin, T.; Huang, P. Measured behaviors of an oversized irregular basement excavation and its surrounding responses in thick soft clay. *Arab. J. Geosci.* **2019**, *13*, 3. [[CrossRef](#)]
19. Liu, Y.; Xiang, B.; Fu, M. Observed Performance of a Large-Scale Deep Triangular Excavation in Shanghai Soft Clays. *Geotech. Geol. Eng.* **2019**, *37*, 2791–2809. [[CrossRef](#)]
20. Ren, D.; Kang, C.; Liu, H.; Li, Y.; Wang, J. Characteristics of a Large-Scale Deep Foundation Pit Excavated by the Central-Island Technique in Chengdu Soft Clay. *KSCE J. Civ. Eng.* **2022**, *26*, 2610–2623. [[CrossRef](#)]
21. Liang, R.; Wu, J.; Sun, L.; Shen, W.; Wu, W. Performances of adjacent metro structures due to zoned excavation of a large-scale basement in soft ground. *Tunn. Undergr. Space Technol.* **2021**, *117*, 104123. [[CrossRef](#)]
22. Ho, S.K.; Gao, F. Case Study of Large-Scale Unsupported Excavation. *Sino-Geotech.* **2011**, *128*, 89–98.
23. Liao, N.-H. Application of Empirical Soil Parameters in Numerical Analysis. Master's Thesis, National Cheng Kung University, Tainan, Taiwan, 2003.
24. Ou, C.-Y. *Deep Excavation Engineering: Analysis, Design Theories and Practices*; Science and Technology Books: Taipei, Taiwan, 2002.
25. Wu, P.-Z.; Wang, M.-J.; Peng, Y.-R. Investigation of Continuous Wall Deformation Behavior. In Proceedings of the 7th Geotechnical Engineering Research Symposium, Berlin, Germany, 8–11 September 1997.

Disclaimer/Publisher's Note: The statements, opinions and data contained in all publications are solely those of the individual author(s) and contributor(s) and not of MDPI and/or the editor(s). MDPI and/or the editor(s) disclaim responsibility for any injury to people or property resulting from any ideas, methods, instructions or products referred to in the content.